ARMY RESEARCH LABORATORY

Failure Analysis of OH-58 Kiowa Warrior Drive Gear Shafts

by Scott Grendahl, Victor Champagne, and Dan Snoha

ARL-TR-3827 **June 2006**

prepared by

U.S. Army Research Laboratory
Weapons and Materials Research Directorate
Aberdeen Proving Ground, MD 21005-5069

for

U.S. Army Research, Development, and Engineering Command
Aviation Engineering Directorate
Propulsion Division
Aberdeen Proving Ground, MD 21010-5424

NOTICES

Disclaimers

The findings in this report are not to be construed as an official Department of the Army position unless so designated by other authorized documents.

Citation of manufacturer's or trade names does not constitute an official endorsement or approval of the use thereof.

Destroy this report when it is no longer needed. Do not return it to the originator.

Army Research Laboratory
Aberdeen Proving Ground, MD 21005-5069

ARL-TR-3827 **June 2006**

Failure Analysis of OH-58 Kiowa Warrior Drive Gear Shafts

Scott Grendahl, Victor Champagne, and Dan Snoha
Weapons and Materials Research Directorate, ARL

prepared by

U.S. Army Research Laboratory
Weapons and Materials Research Directorate
Aberdeen Proving Ground, MD 21005-5069

for

U.S. Army Research, Development, and Engineering Command
Aviation Engineering Directorate
Propulsion Division
Aberdeen Proving Ground, MD 21010-5424

REPORT DOCUMENTATION PAGE

Form Approved
OMB No. 0704-0188

1. REPORT DATE *(DD-MM-YYYY)*	2. REPORT TYPE	3. DATES COVERED (From - To)
June 2006	Final	1 January 2005–31 August 2005

4. TITLE AND SUBTITLE
Failure Analysis of OH-58 Kiowa Warrior Drive Gear Shafts

5a. CONTRACT NUMBER

5b. GRANT NUMBER

5c. PROGRAM ELEMENT NUMBER

Scott Grendahl, Victor Champagne, and Dan Snoha

5d. PROJECT NUMBER
M042-489Y31

5e. TASK NUMBER

5f. WORK UNIT NUMBER

7. PERFORMING ORGANIZATION NAME(S) AND ADDRESS(ES)
U.S. Army Research Laboratory
ATTN: AMSRD-ARL-WM-MC
Aberdeen Proving Ground, MD 21005-5069

8. PERFORMING ORGANIZATION REPORT NUMBER
ARL-TR-3827

9. SPONSORING/MONITORING AGENCY NAME(S) AND ADDRESS(ES)
U.S. Army Research, Develoment, and Engineering Command
Aviation Engineering Directorate
Propulsion Division
Aberdeen Proving Ground, MD 21010-5424

10. SPONSOR/MONITOR'S ACRONYM(S)

11. SPONSOR/MONITOR'S REPORT NUMBER(S)

12. DISTRIBUTION/AVAILABILITY STATEMENT
Approved for public release; distribution is unlimited.

13. SUPPLEMENTARY NOTES

14. ABSTRACT

A 15-hp spare drive gear from a 250-C30/R3 engine on an OH-58 Kiowa Warrior failed in service, causing loss of AC power. The failed gear, all recovered teeth, and the driving pinion were sent to the U.S. Army Research Laboratory for investigation. This investigation focused on determining the mode of failure and any possible metallurgical or manufacturing contribution to this failure. Analysis included optical and scanning electron microscopy, chemical analysis, and measurements of hardness and surface finish.

15. SUBJECT TERMS
failure analysis, 9310 steel, fatigue, helicopter gear

16. SECURITY CLASSIFICATION OF:			17. LIMITATION OF ABSTRACT	18. NUMBER OF PAGES	19a. NAME OF RESPONSIBLE PERSON
a. REPORT	b. ABSTRACT	c. THIS PAGE			Scott Grendahl
UNCLASSIFIED	UNCLASSIFIED	UNCLASSIFIED	UL	60	19b. TELEPHONE NUMBER (*Include area code*) 410-306-0819

Contents

List of Figures

List of Tables

INTENTIONALLY LEFT BLANK.

1. Introduction

A 15-hp spare drive gear from a 250-C30/R3 engine on an OH-58 Kiowa Warrior failed in service, causing loss of AC power. The failed gear, all recovered teeth, and the driving pinion were sent to the U.S. Army Research Laboratory for investigation. This investigation focused on determining the mode of failure and any possible metallurgical or manufacturing contribution to this failure. Analysis included optical and scanning electron microscopy, chemical analysis, and measurements of hardness and surface finish.

The objective of this report is root cause determination for the 15-hp spare drive gear failure.

2. Discussion

All teeth were stripped or separated from the failed gear; many fracture surfaces were too marred to yield useful information. Thirteen teeth were recovered essentially intact. The recovered teeth were successfully matched to their corresponding location on the gear by examination of the tooth geometry and fracture topography. The location of each tooth relative to the others is shown in figure 1.

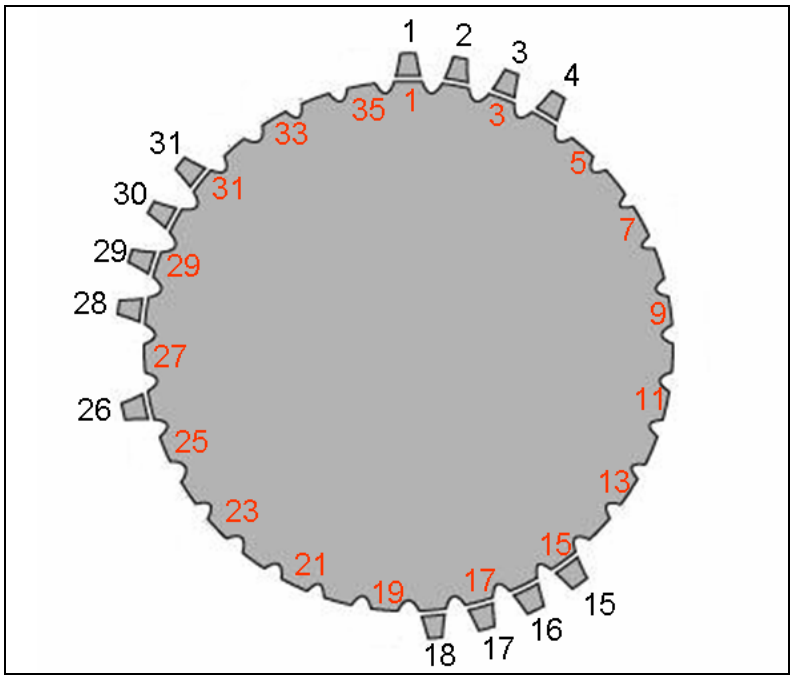

Figure 1. Location of recovered teeth on spare drive gear. (Gear is driven counterclockwise.)

Failure occurs due to very high cycle bending fatigue of the initial tooth. The next tooth in the meshing sequence experiences impact loading due to the momentary loss of contact with the driving pinion. Bending fatigue failure occurs progressively faster for each subsequent tooth. The initial tooth fails in very high cycle fatigue while the last tooth fails in low cycle fatigue. After loss of sufficient teeth, transmission error becomes so large that the gears do not mesh properly, causing rapid failure of the remaining gear teeth and damage to the pinion teeth as well.

Failure order was established by fractographic examination. Optical and scanning electron microscope (SEM) examination of the fracture surfaces support the failure scenario presented.

Two groups of teeth failed sequentially in bending fatigue, teeth 1–4 and teeth 28–31. While it was not possible to determine with absolute certainty which group began to fail first, it is clear that within each group failure occurred in the order stated. Based on the extremely small overload region on tooth 1 (much smaller than that of tooth 28) and fractography it is suspected that group 1–4 began to fail first. It is also clear based on fractography that the two groups were failing simultaneously.

Pit origins were observed at teeth 1, 2, 4, 28, and 30. Prominent tool marks were observed at the origins of teeth 3, 29, and 31.

3. Optical Microscopy

Components were examined optically using a Nikon SMZ-1500 zoom stereo microscope. Particular attention was given to fracture morphology and wear on both the failed gear and mating pinion.

Facture surfaces for tooth 1 are shown in figures 2–5. The primary origin for this tooth is shown in figure 4. Propagation was by fatigue with a secondary crack initiating on the coast side. A very small overload region was present, as depicted in figure 5.

Figures 6 (tooth half) and 7 (gear half) show the fracture surfaces observed on tooth 2. Note the more pronounced beach marks relative to tooth 1.

Figures 8 and 9, respectively, present the tooth and gear fracture halves of tooth 3. The overload region was significantly larger than on the preceding teeth.

The fracture halves of tooth 4 are presented in figure 10 (tooth half) and figure 11 (gear half). The beachmarks exhibited a “U” or bathtub shape. A large mound can be seen in figure 10; the mating cavity can be seen in figure 11.

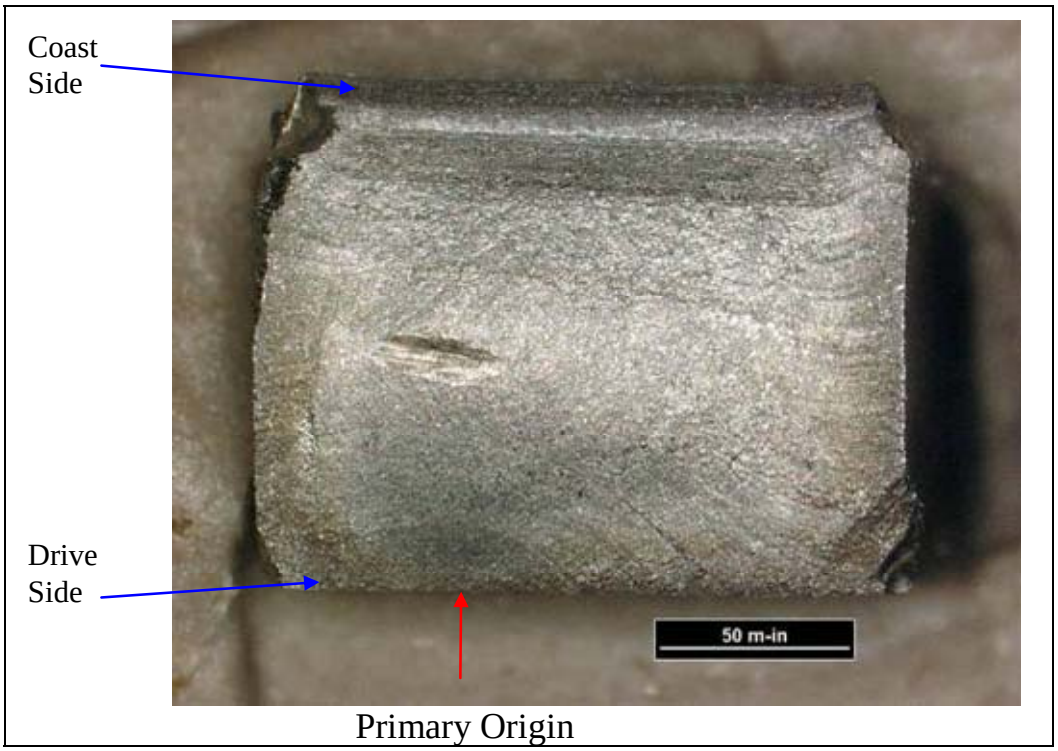

Figure 2. Tooth 1, tooth fracture half.

Figure 3. Tooth 1, gear fracture half.

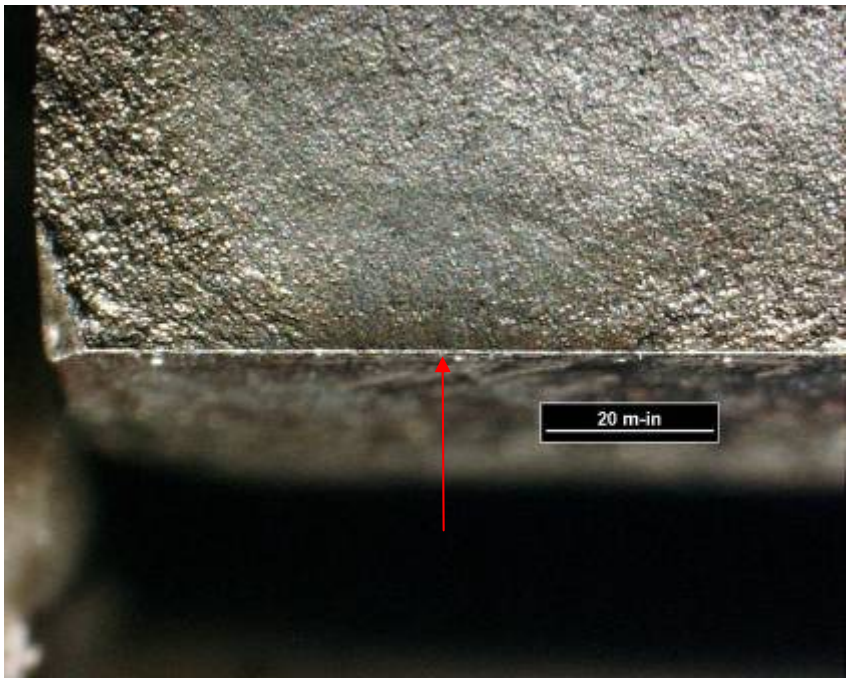

Figure 4. Primary origin, drive side of tooth 1, tooth fracture half.

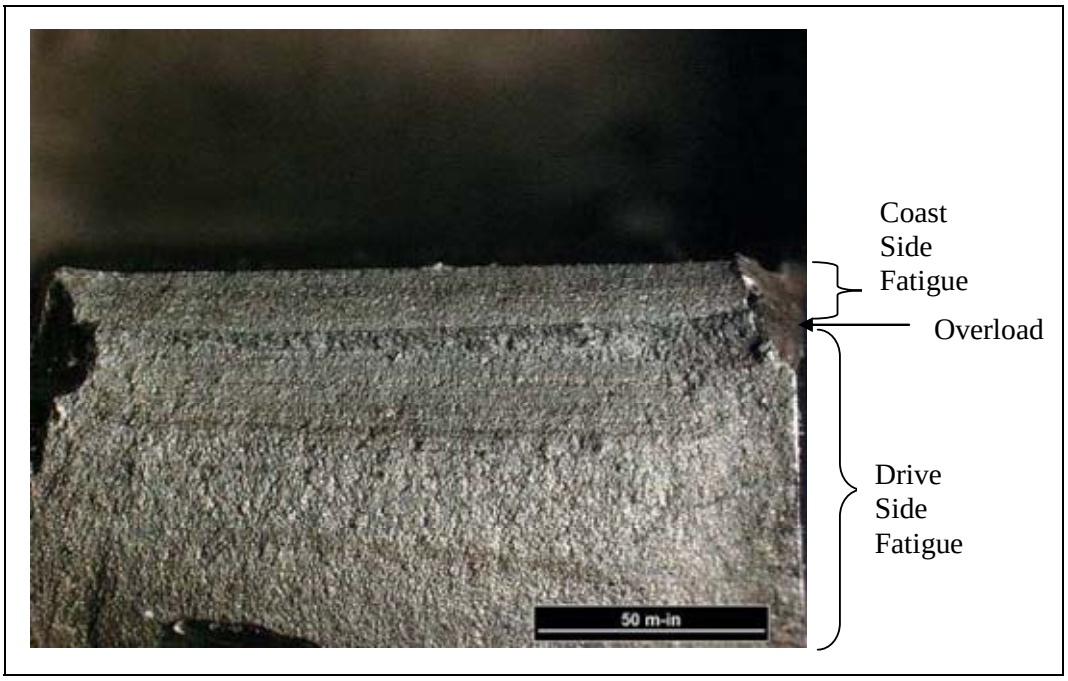

Figure 5. Coast side of tooth 1, tooth fracture half.

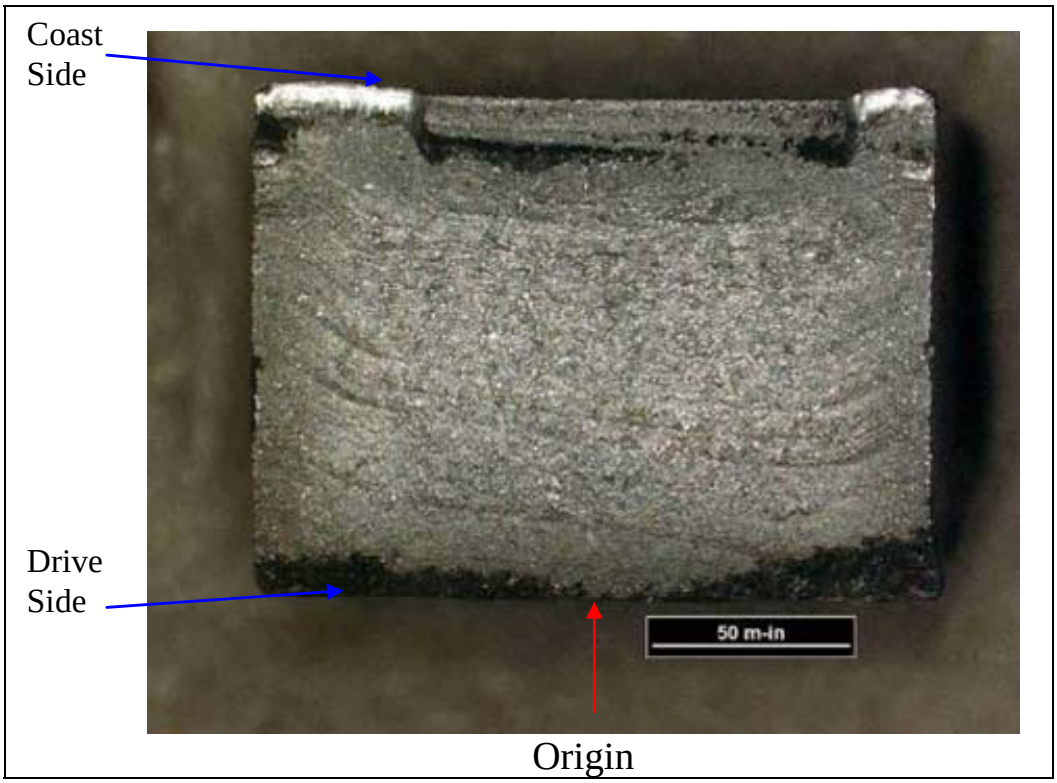

Figure 6. Tooth 2, tooth fracture half.

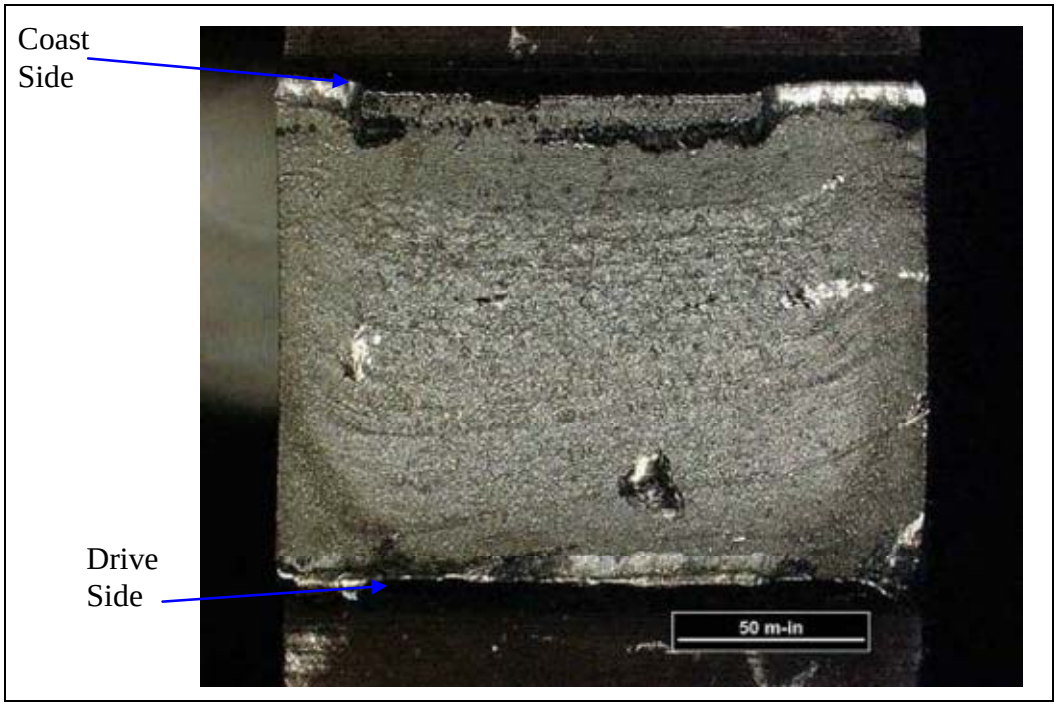

Figure 7. Tooth 2, gear fracture half.

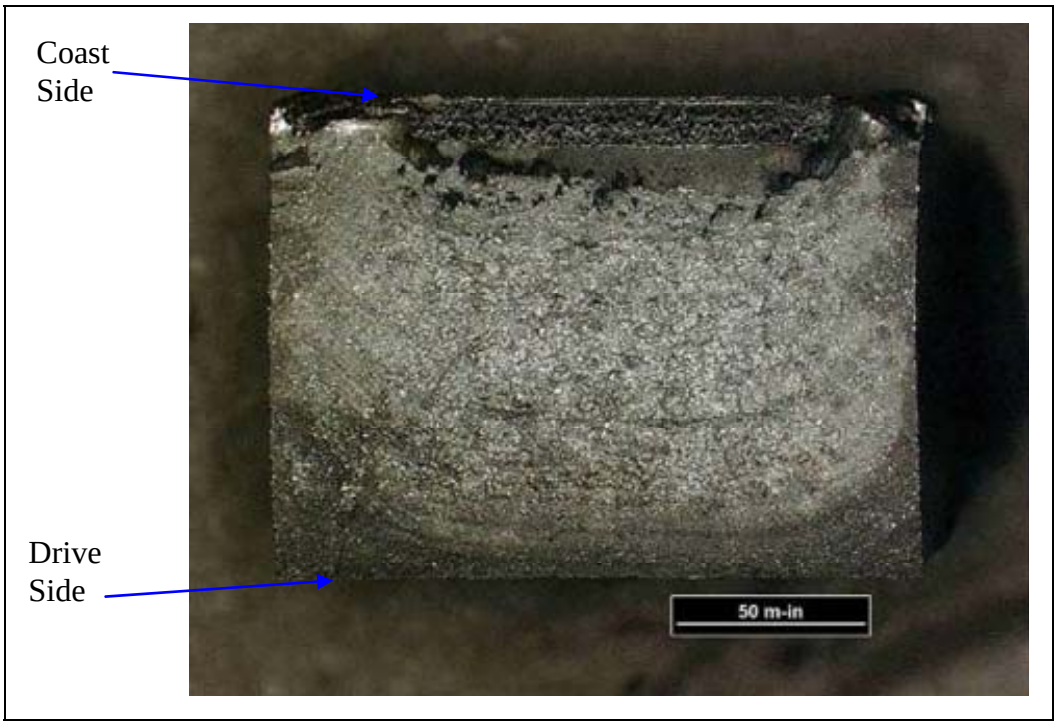

Figure 8. Tooth 3, tooth fracture half.

Figure 9. Tooth 3, gear fracture half.

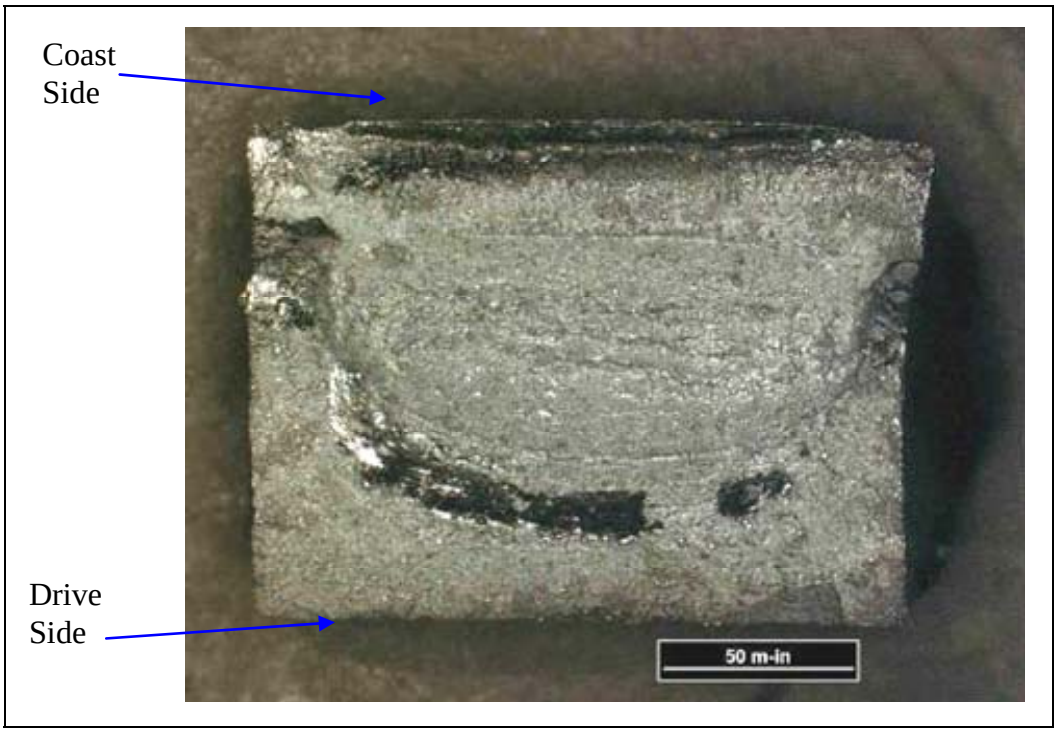

Figure 10. Tooth 4, tooth fracture half.

Figure 11. Tooth 4, gear fracture half.

The second group, teeth 28–31, failed in a similar manner. All teeth failed in bending fatigue, originating in the drive side root.

The primary failure for this group was tooth 28. The fracture halves are shown in figures 12 and 13. As in tooth 1, a secondary crack originated on the coast side. A small overload region was present.

Tooth 29 fracture halves are shown in figures 14 and 15. Fracture halves for tooth 30 are shown in figures 16 and 17.

Figures 18 and 19 present the fracture halves for tooth 31. Wear was present at the drive side origin for this tooth (figures 26–28). Note that this was the last tooth in this sequence to fail by bending fatigue.

Figures 20–28 are representative of the wear pattern observed on most of the teeth recovered.

Prominent tool marks were observed in the roots of the gear teeth, as shown in figures 29–30. Depth of the typical tool marks measured was 0.0001–0.0002 in (figures 31 and 32).

Figures 33 and 34 show the drive and coast sides of the mating pinion. Note that the wear pattern is offset, as the spare drive gear is not centered with respect to the pinion.

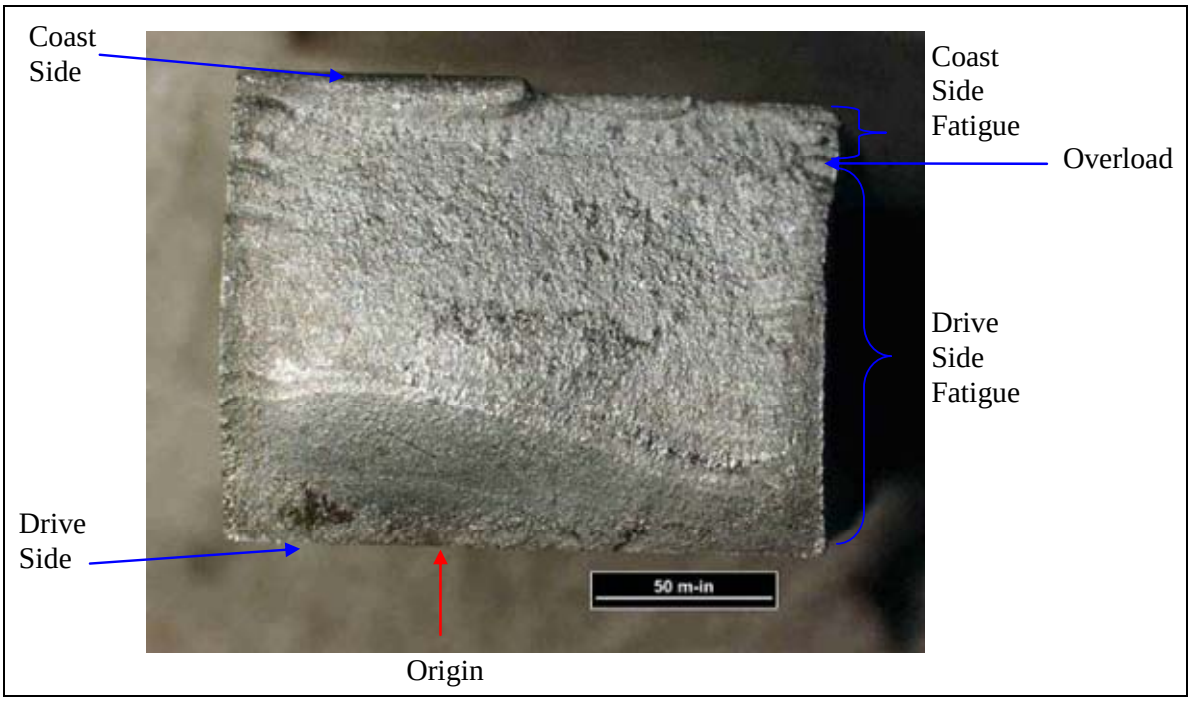

Figure 12. Tooth 28, tooth fracture half.

Figure 13. Tooth 28, gear fracture half.

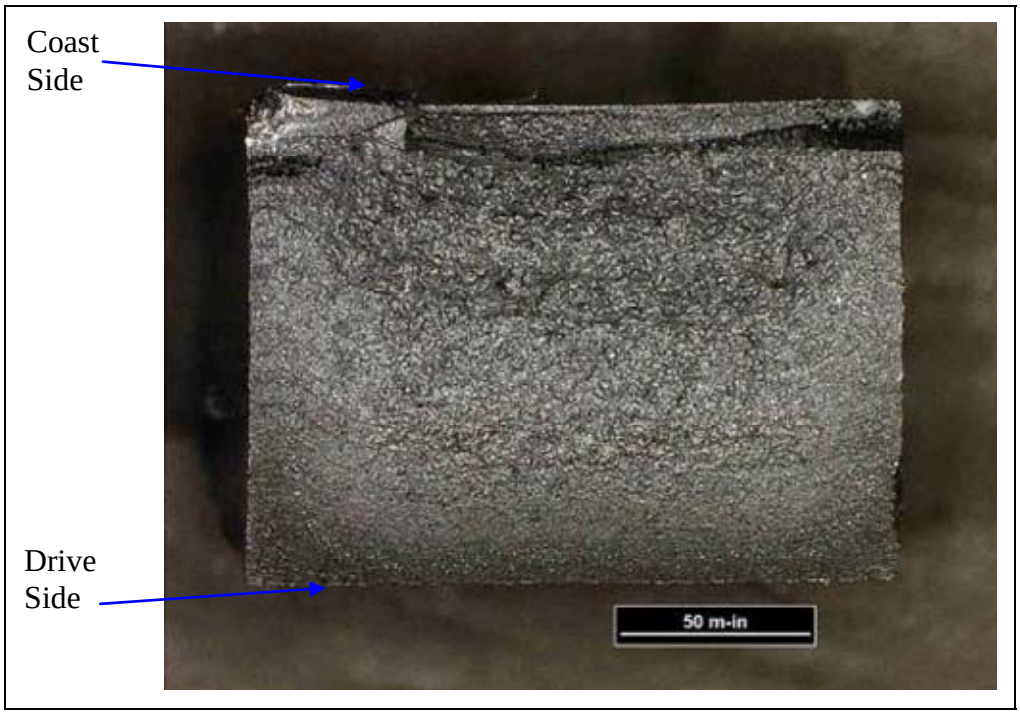

Figure 14. Tooth 29, tooth fracture half.

Figure 15. Tooth 29, gear fracture half.

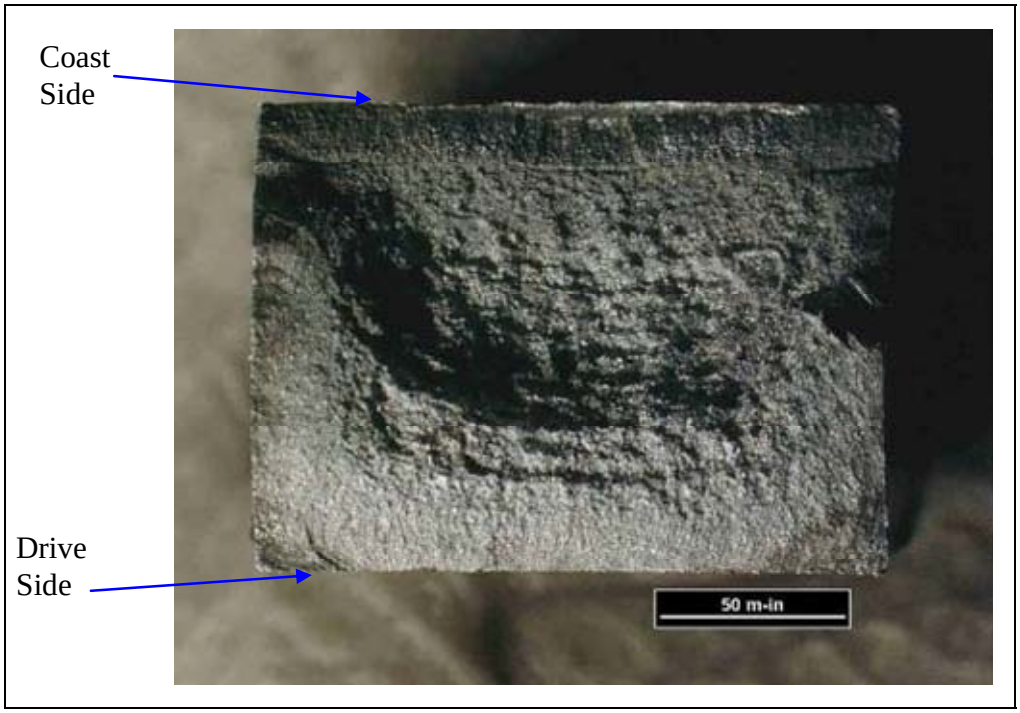

Figure 16. Tooth 30, tooth fracture half.

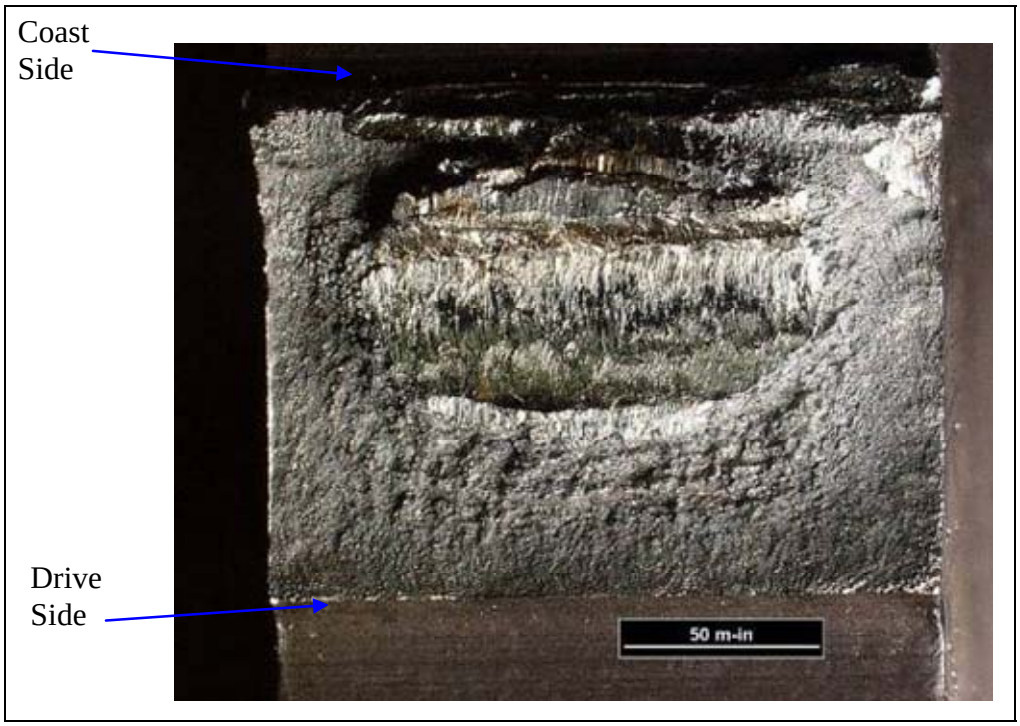

Figure 17. Tooth 30, gear fracture half.

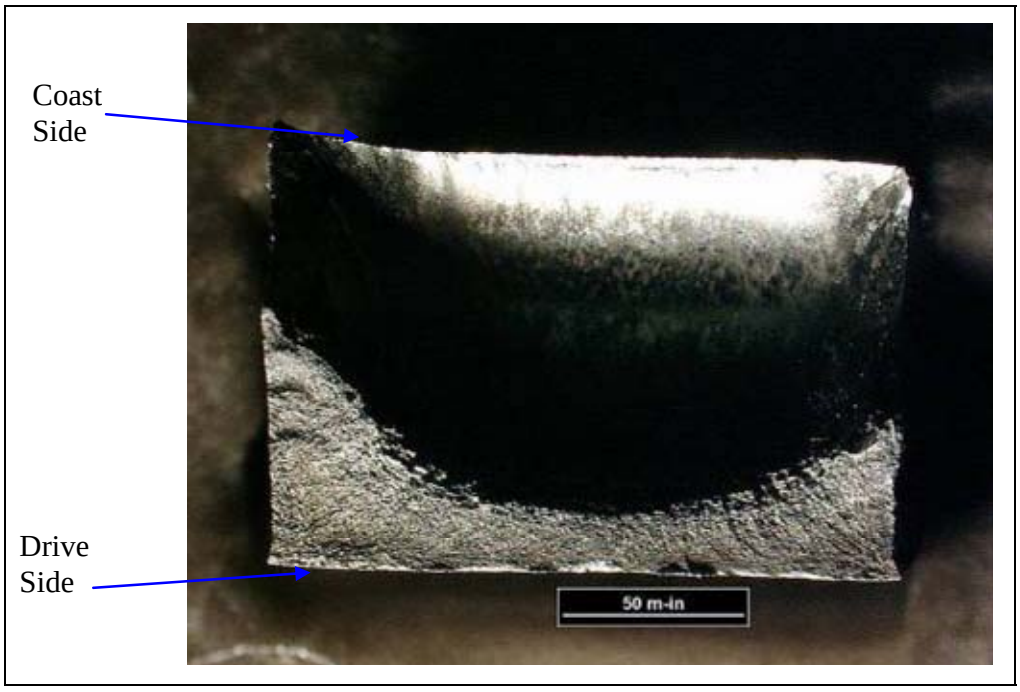

Figure 18. Tooth 31, tooth fracture half.

Figure 19. Tooth 31, gear fracture half.

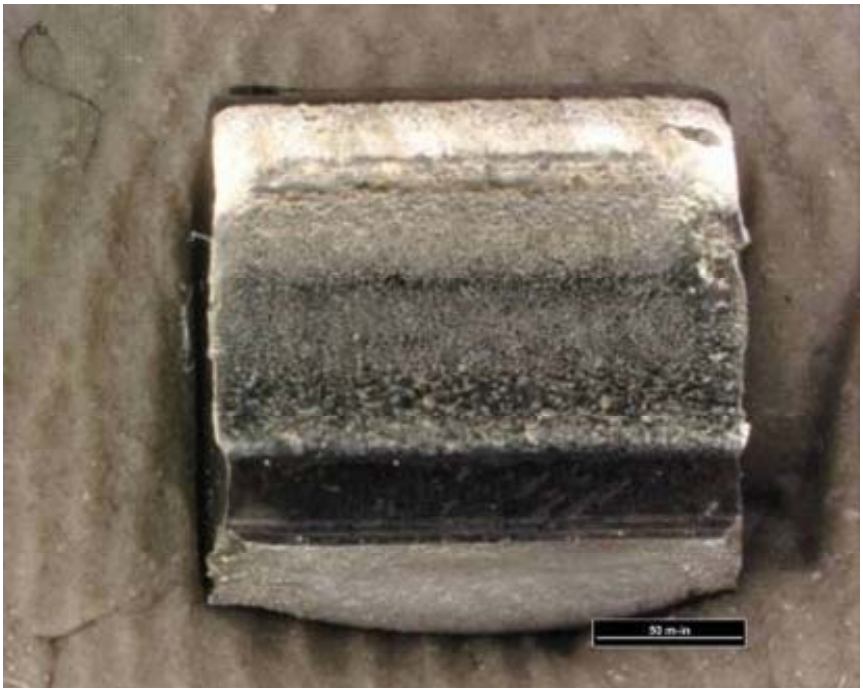

Figure 20. Drive side, tooth 1.

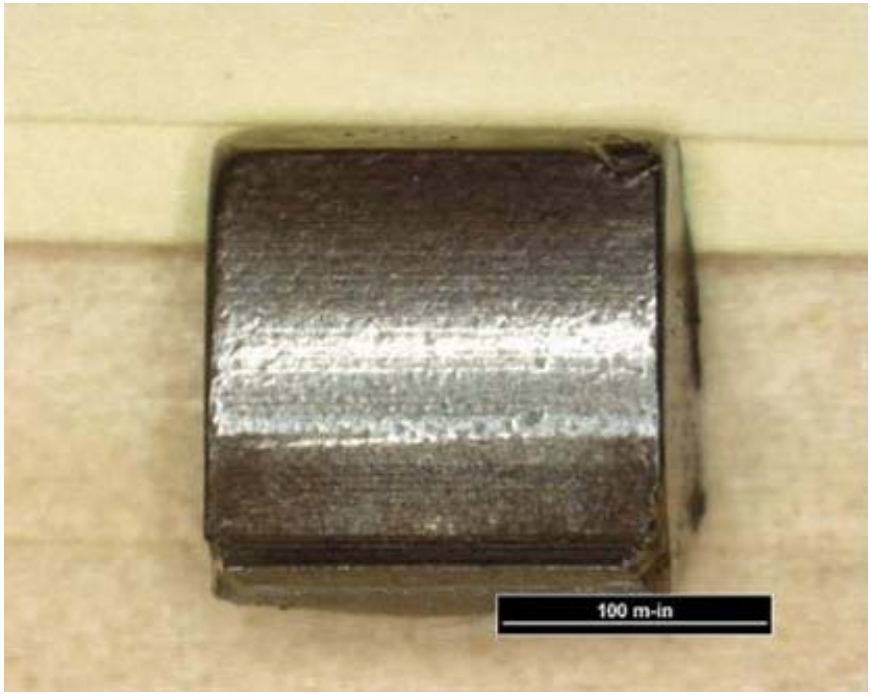

Figure 21. Coast side wear, tooth 1.

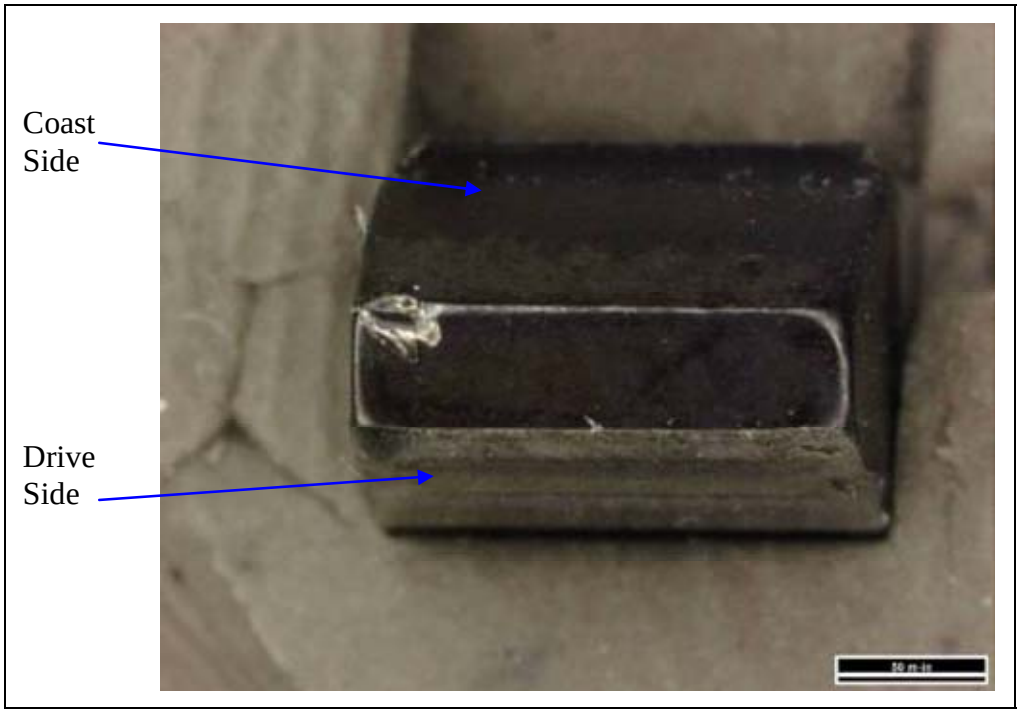

Figure 22. Top of tooth 1.

Figure 23. Drive side, tooth 18.

Figure 24. Coast side, tooth 18.

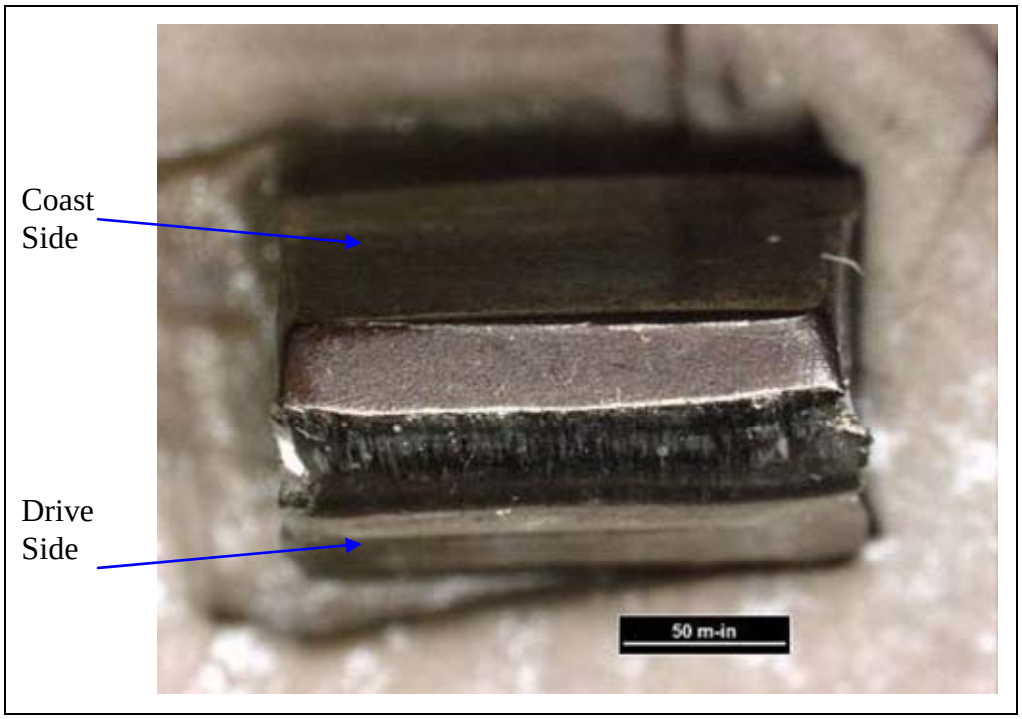

Figure 25. Top of tooth 18.

Figure 26. Drive side, tooth 31. (Note: worn adjacent to fracture surface.)

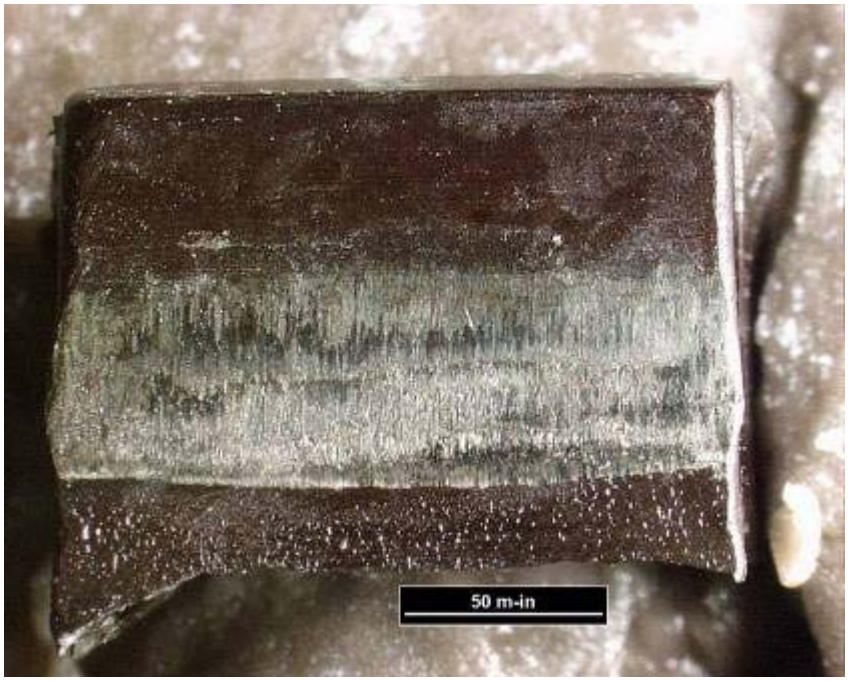

Figure 27. Coast side, tooth 31.

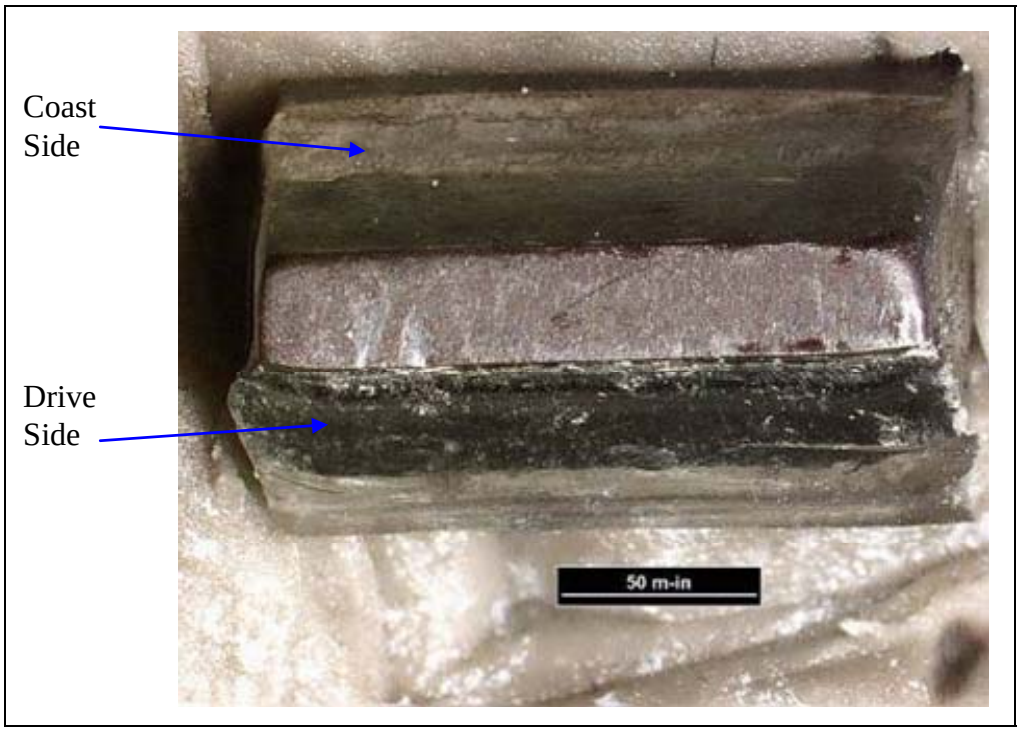

Figure 28. Top of tooth 31.

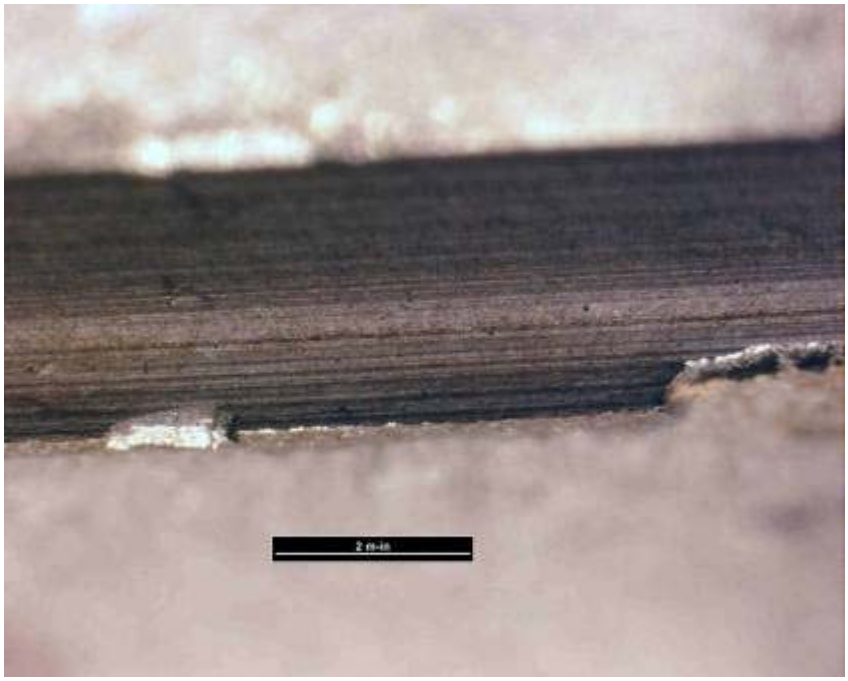

Figure 29. Typical tool marks, tooth root fillet, between teeth 15 and 16.

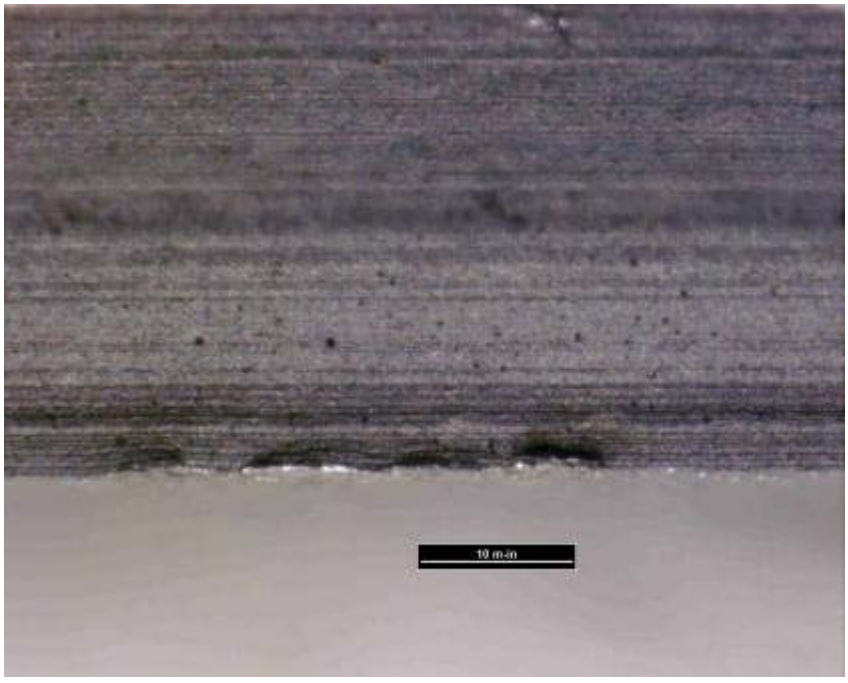

Figure 30. Typical tool marks, tooth root fillet, between teeth 16 and 17.

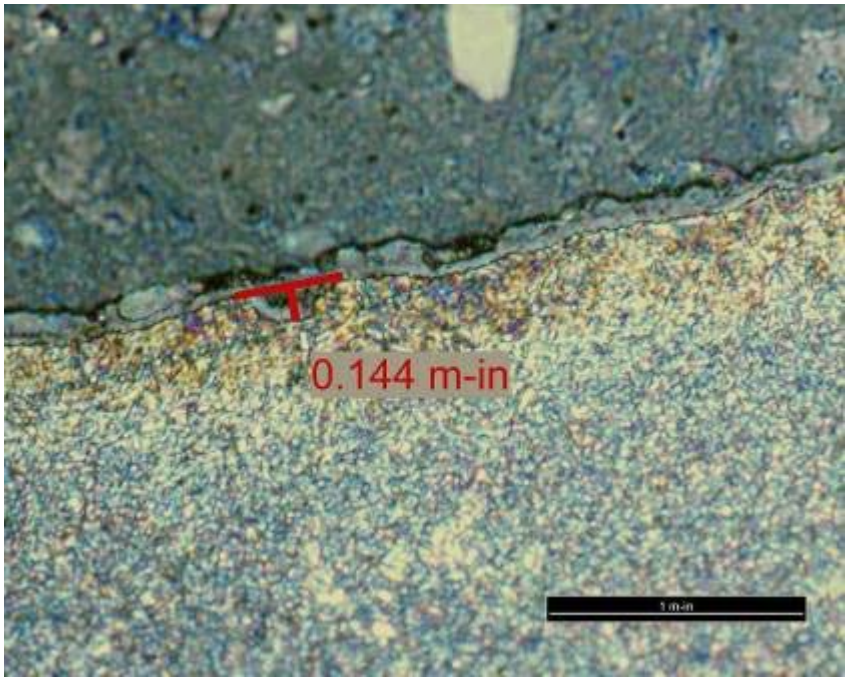

Figure 31. Typical tool mark depth, tooth root, measurement no. 1.

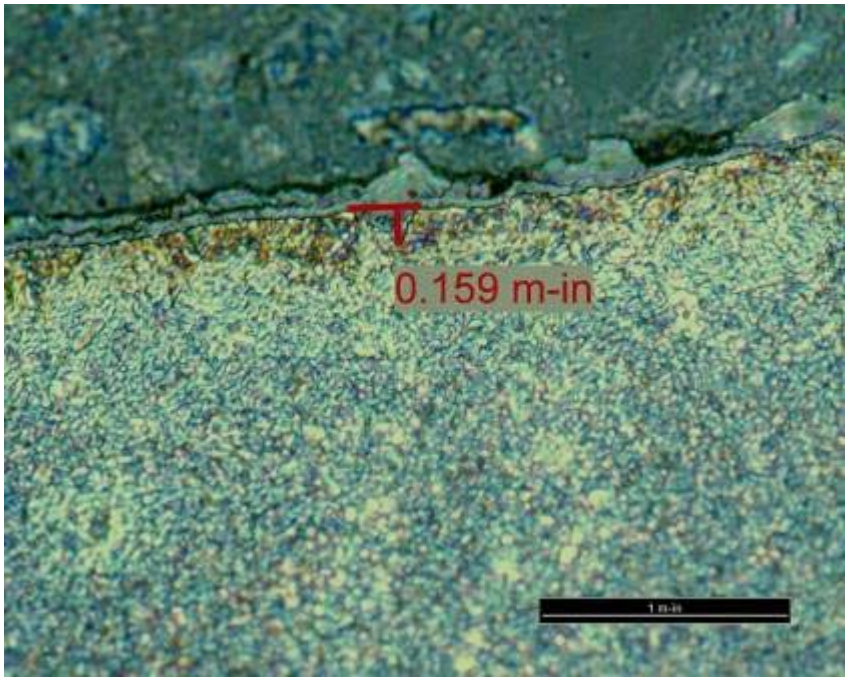

Figure 32. Typical tool mark depth, tooth root, measurement no. 2.

Figure 33. Drive side idler gear.

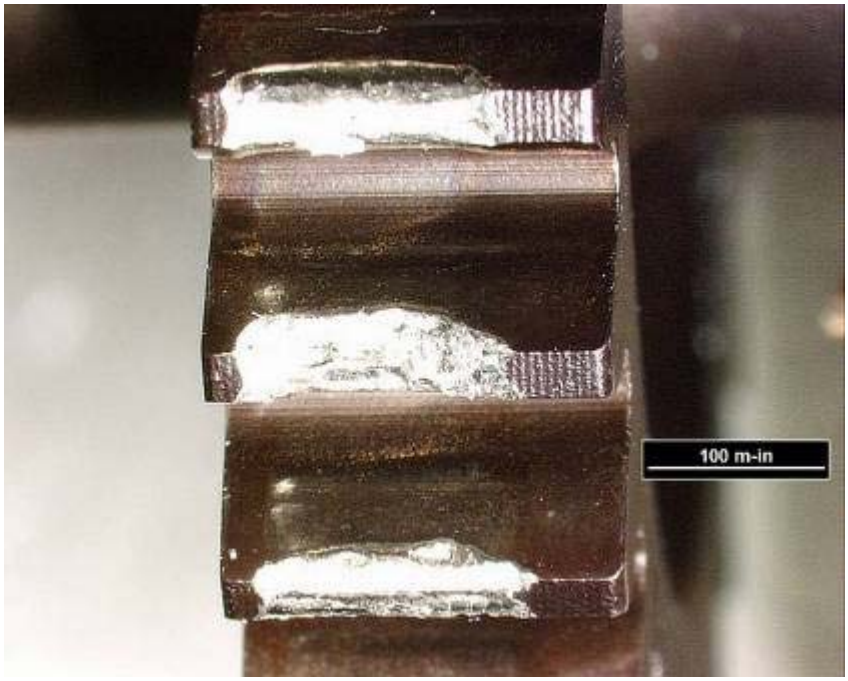

Figure 34. Coast side idler gear.

4. Scanning Electron Microscopy

Scanning electron microscopy was performed on all 13 teeth in a JEOL 6460LV SEM. The SEM investigation focused on fracture surface morphology and on features of interest at the origin. This work confirmed observations made in the optical examination.

Figures 35–41 show SEM micrographs of tooth 1. Figures 36–38 present the origin for this primary failure. The pit origin can be clearly seen in figure 38. A separate crack originated from the coast side of the tooth and can be observed in figures 35 and 41. The two fractures connected through a small (100–150 μm) overload region as shown in figure 41.

The pit origin for tooth 2 can be clearly seen in figure 42, which shows the tooth half of the fracture. Post fracture damage destroyed the gear half origin, depicted in figure 43.

The origin for tooth 3 is shown in figure 44. Initiation appears to occur along a prominent tool mark.

Tooth 4 had multiple origin sites (both pits and tool marks), which are shown in figures 45–47. There was a pit that led to cracking that can be observed on both the tooth and gear fracture halves (figures 45 and 46).

Tooth 28 is shown in figures 48–52. The fracture was remarkably similar to tooth 1; both fractures possessed a primary pit origin (drive side), initiation and propagation from the coast side, and a very small overload region. Figures 49–51 show the origin of fatigue on this primary failure that can be traced to a line of pits including the pit which initiated failure.

Figures 53–58 show the fracture surfaces associated with tooth 29. Failure originated at multiple points along the drive side, which are seen on both the tooth and gear fracture halves, including both pits and tool marks.

Tooth 30 is shown in figures 59–63. Multiple origins were found on the drive side, shown in figures 60–61.

The fracture surface generated by the low cycle fatigue failure of tooth 31 is presented in figure 64. The drive side origin is shown in figure 65. The fracture morphology includes a small amount of mixed mode fracture (figure 66), but is dominated by cyclic overload in the middle of the tooth (figure 67) and near the coast side (figure 68).

Cracking originating from coast side tool marks is shown in figures 69–75.

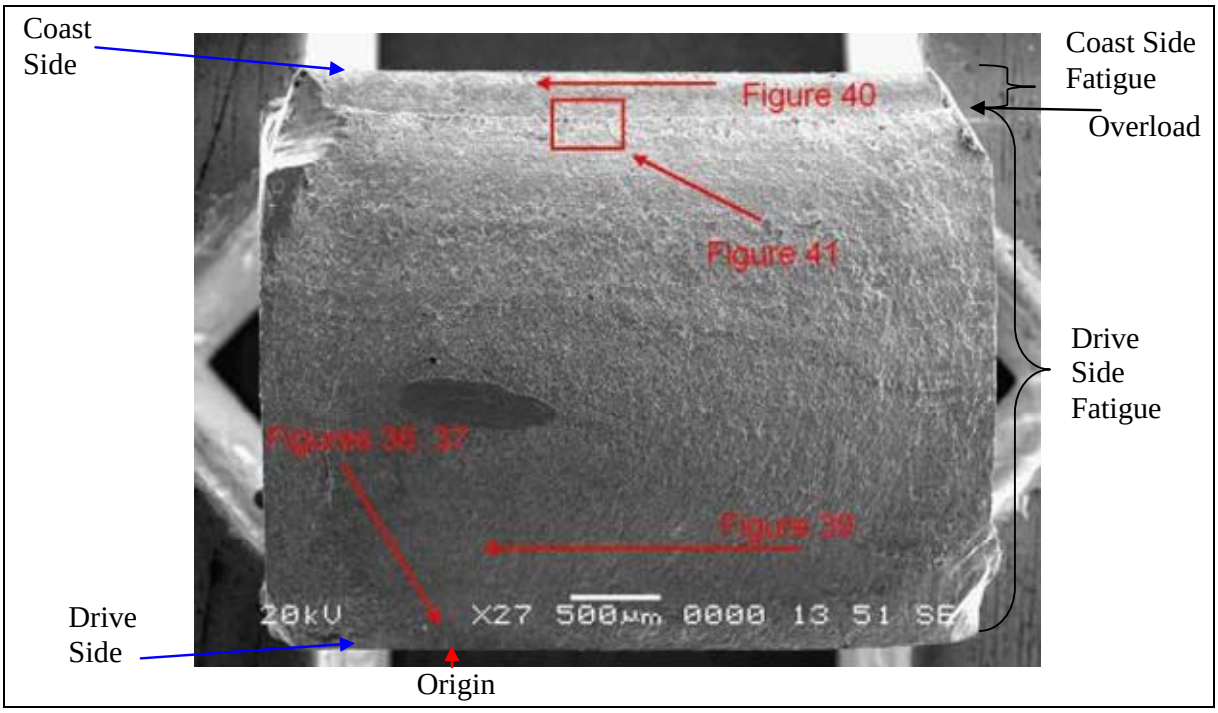

Figure 35. Tooth 1.

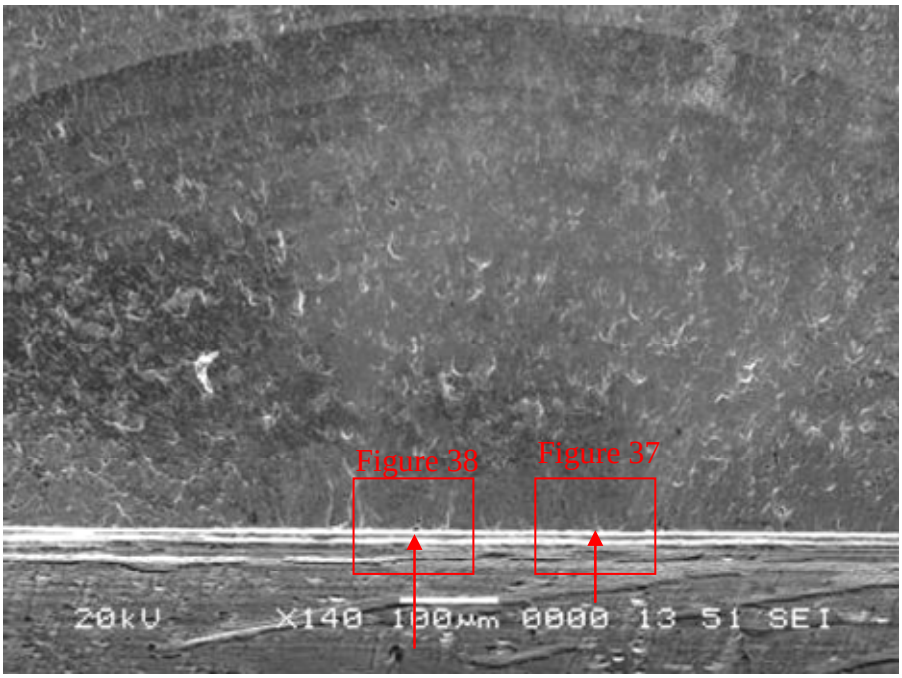

Figure 36. Tooth 1 drive side origin.

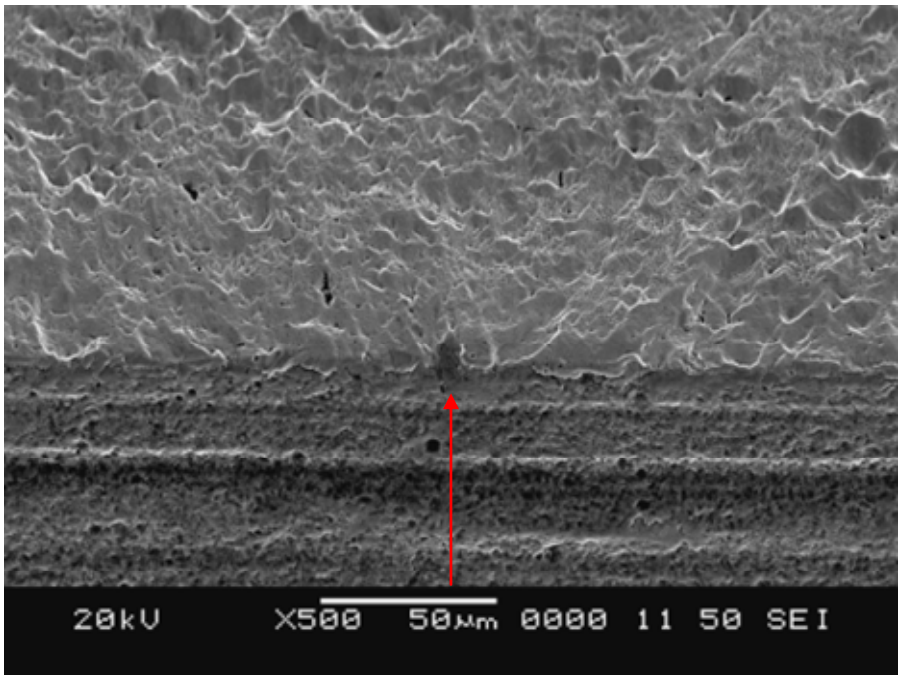

Figure 37. Tooth 1 drive side pit origin site.

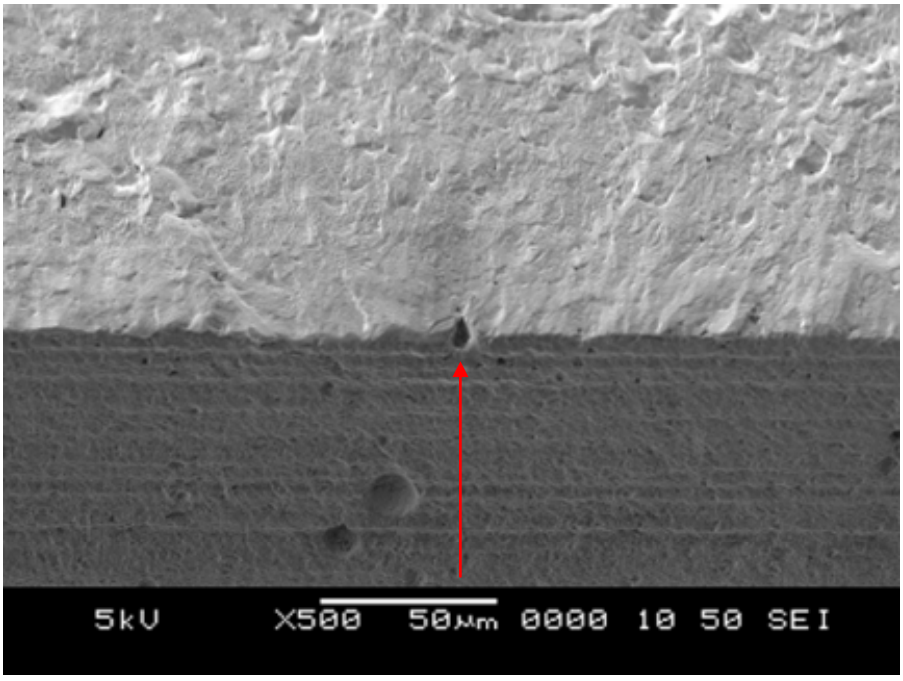

Pit Origin

Figure 38. Tooth 1 primary origin, drive side gear fracture half.

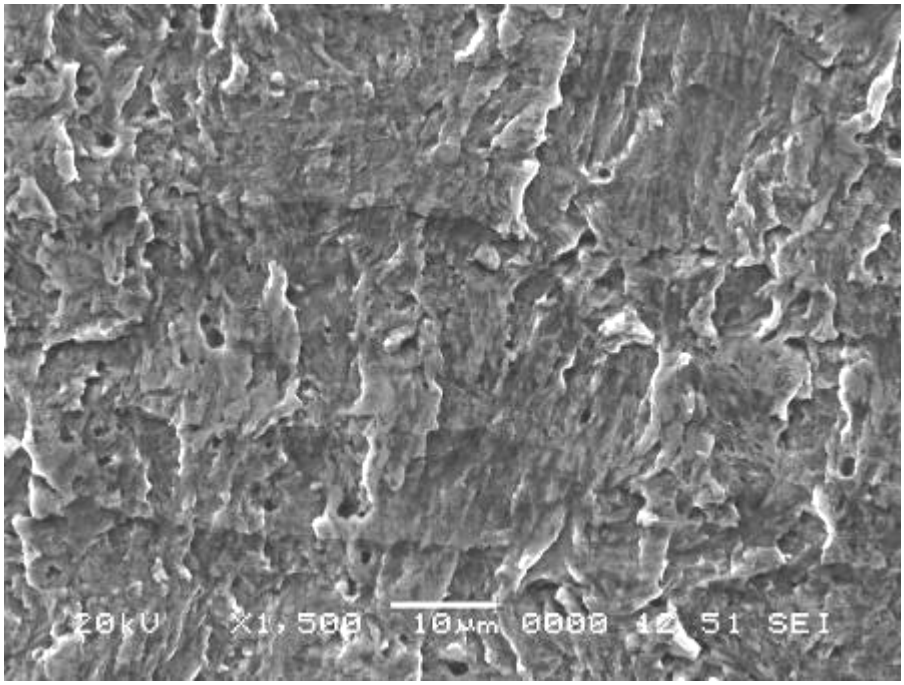

Figure 39. Transgranular morphology, tooth 1 drive side.

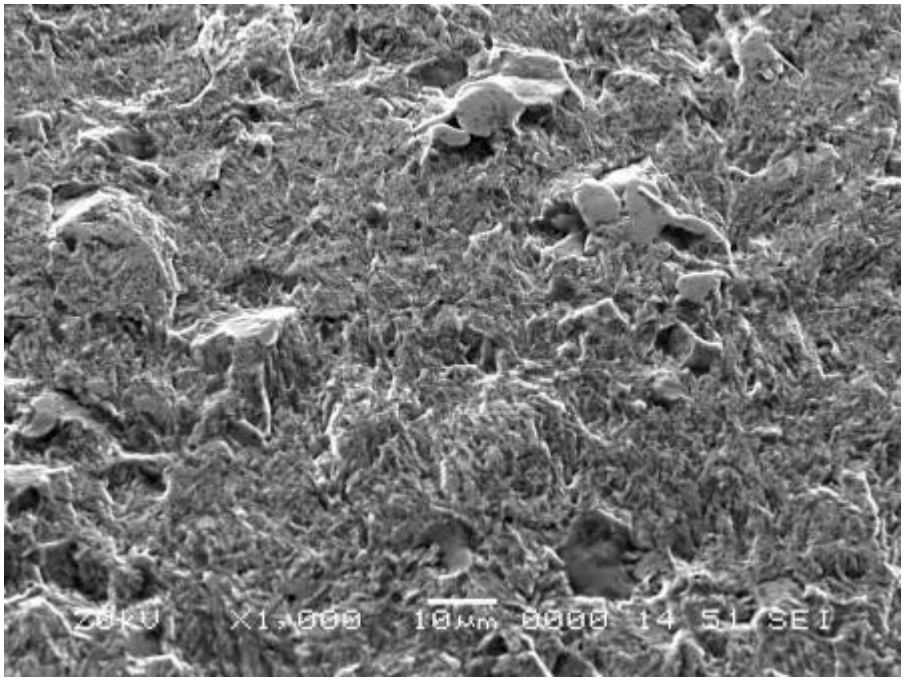

Figure 40. Transgranular morphology, tooth 1 coast side.

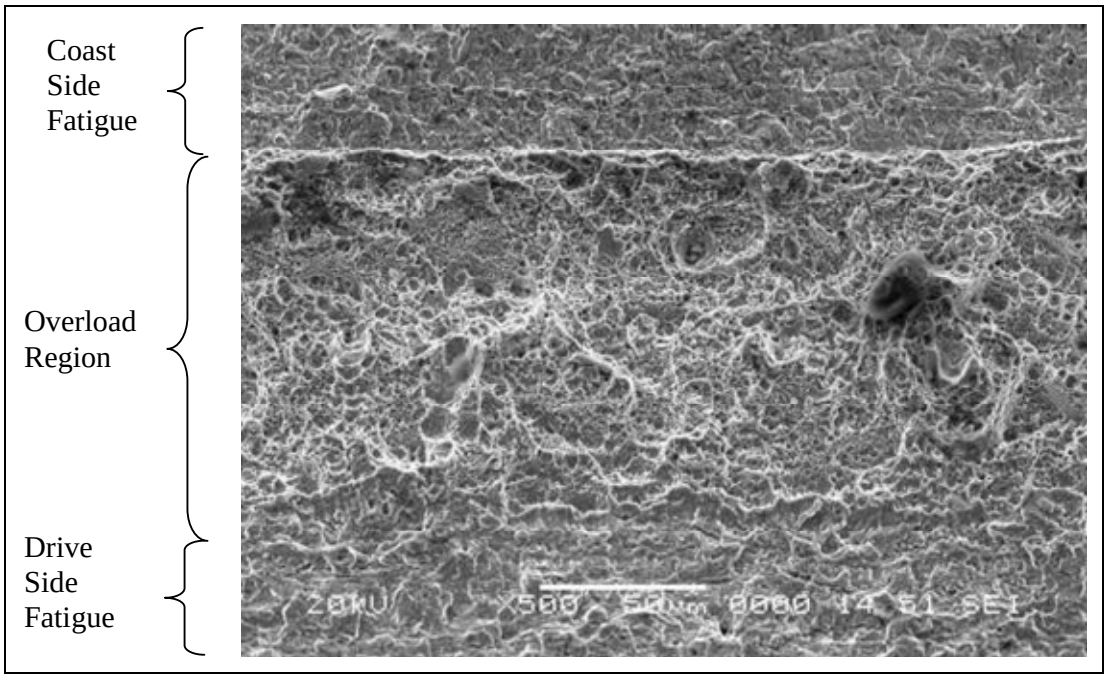

Figure 41. Overload transition, tooth 1.

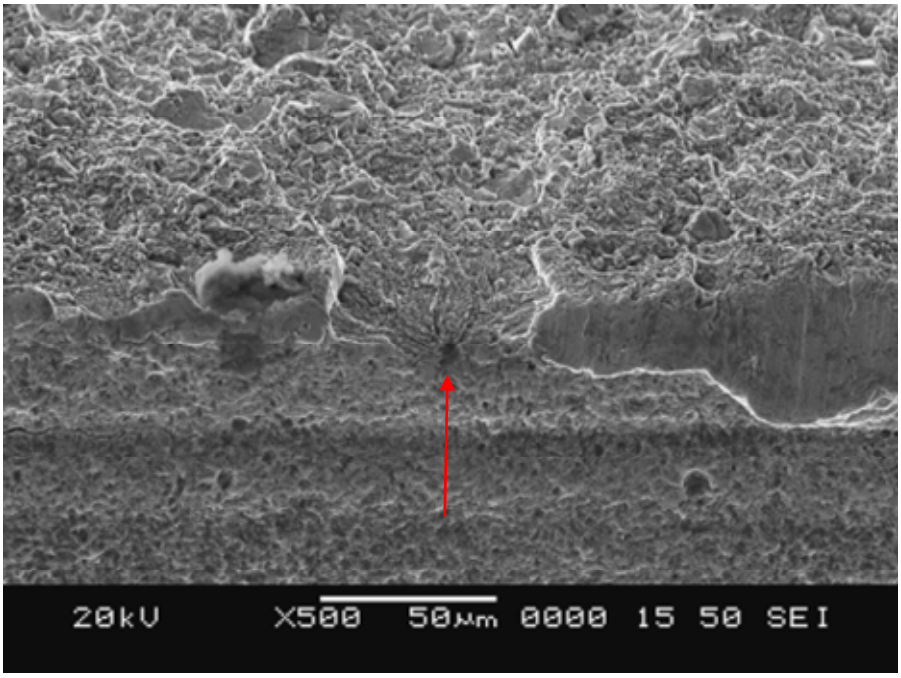

Figure 42. Tooth 2 drive side primary pit origin, tooth half.

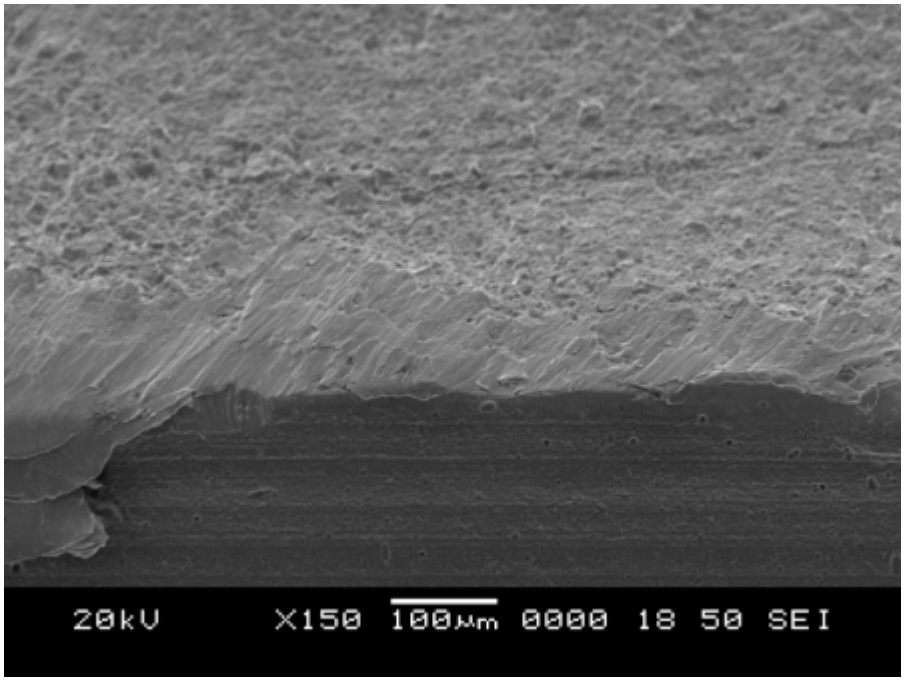

Figure 43. Drive side, tooth 2, gear half, origin location. (Note the damage.)

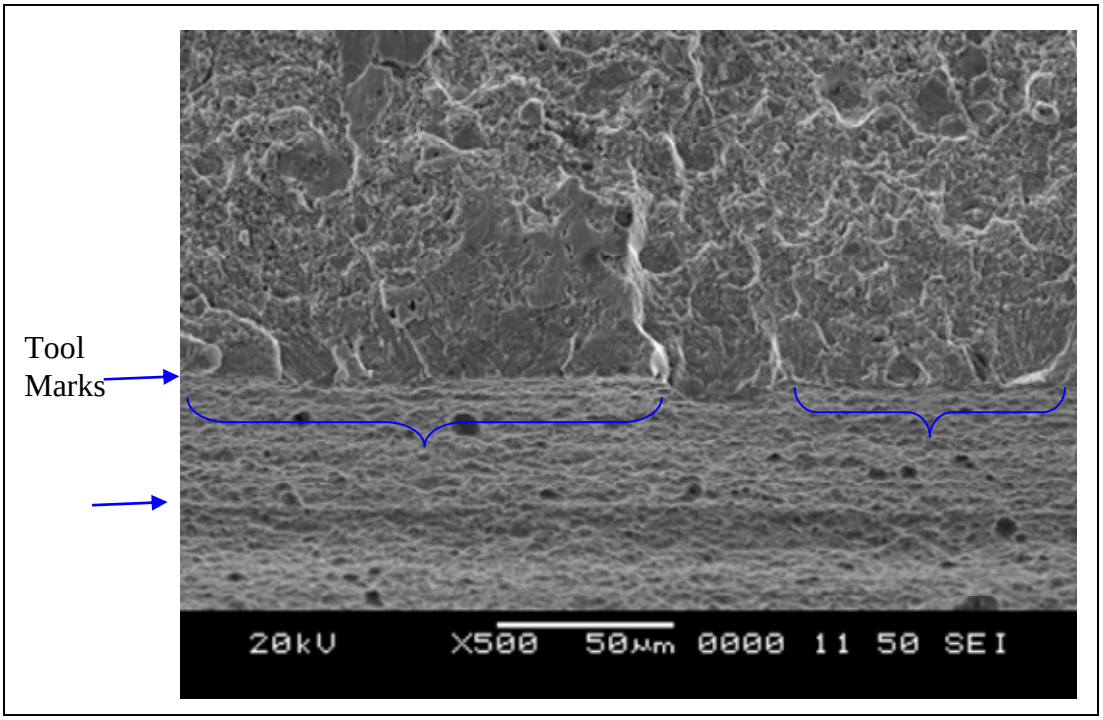

Figure 44. Drive side, tooth 3, primary origin gear half.

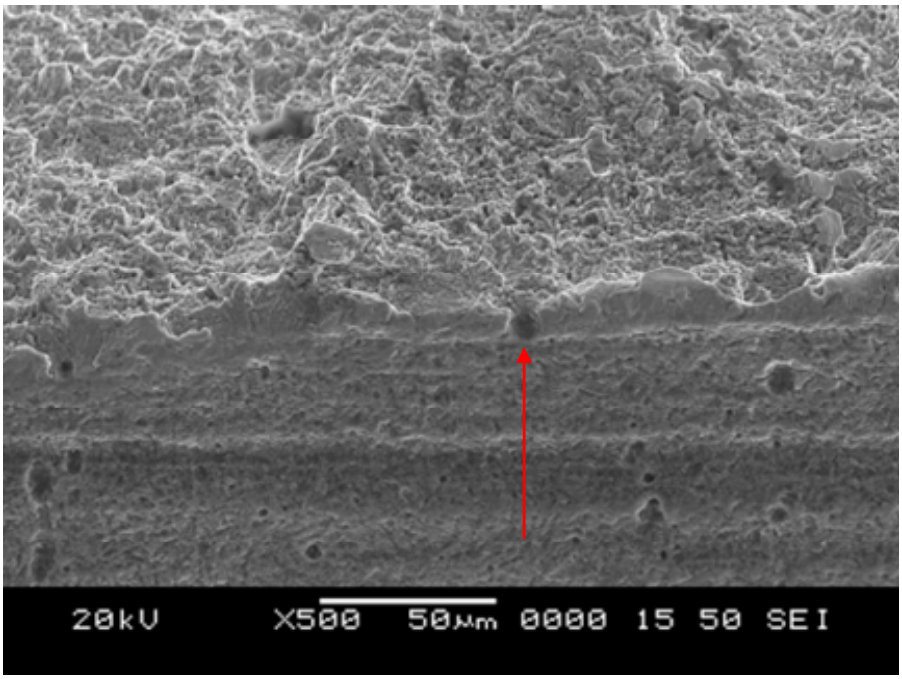

Figure 45. Tooth 4 drive side primary pit origin.

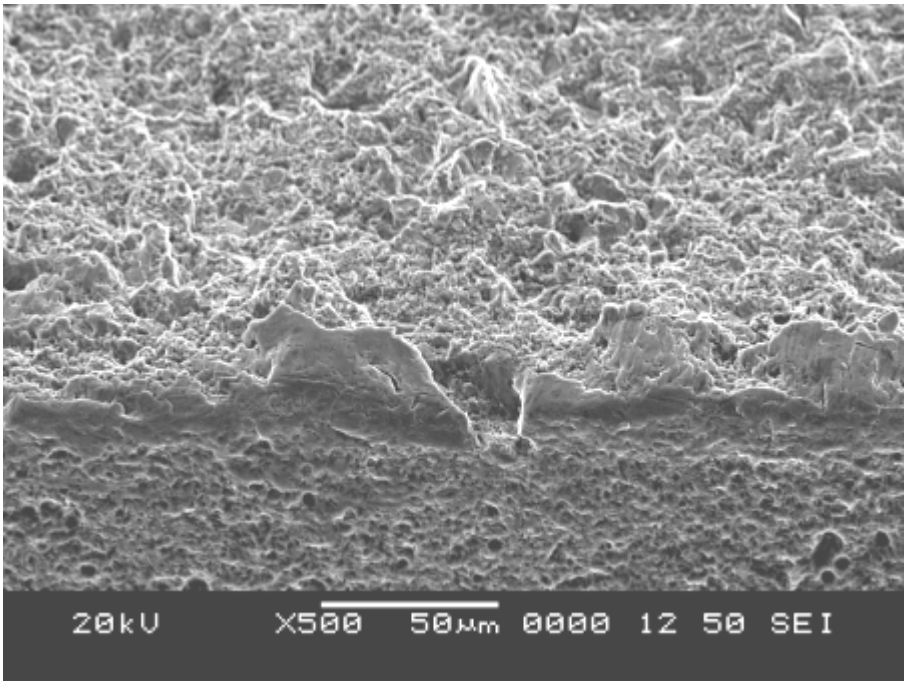

Figure 46. Tooth 4 drive side primary pit origin, gear fracture half.

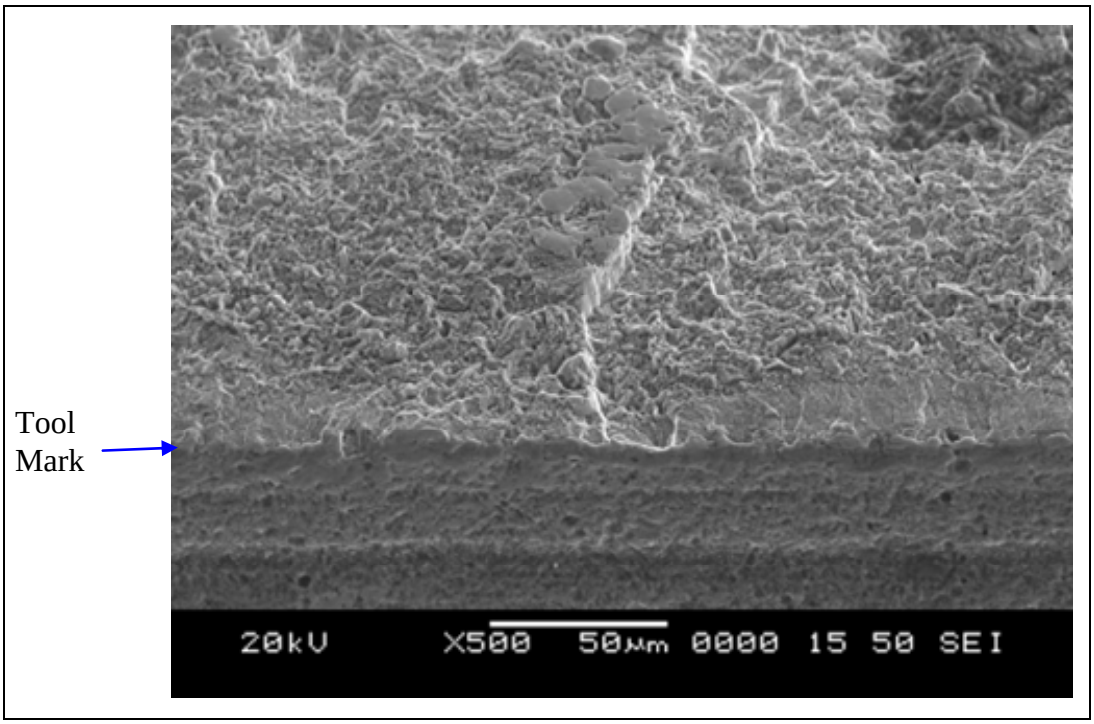

Figure 47. Tooth 4 drive side.

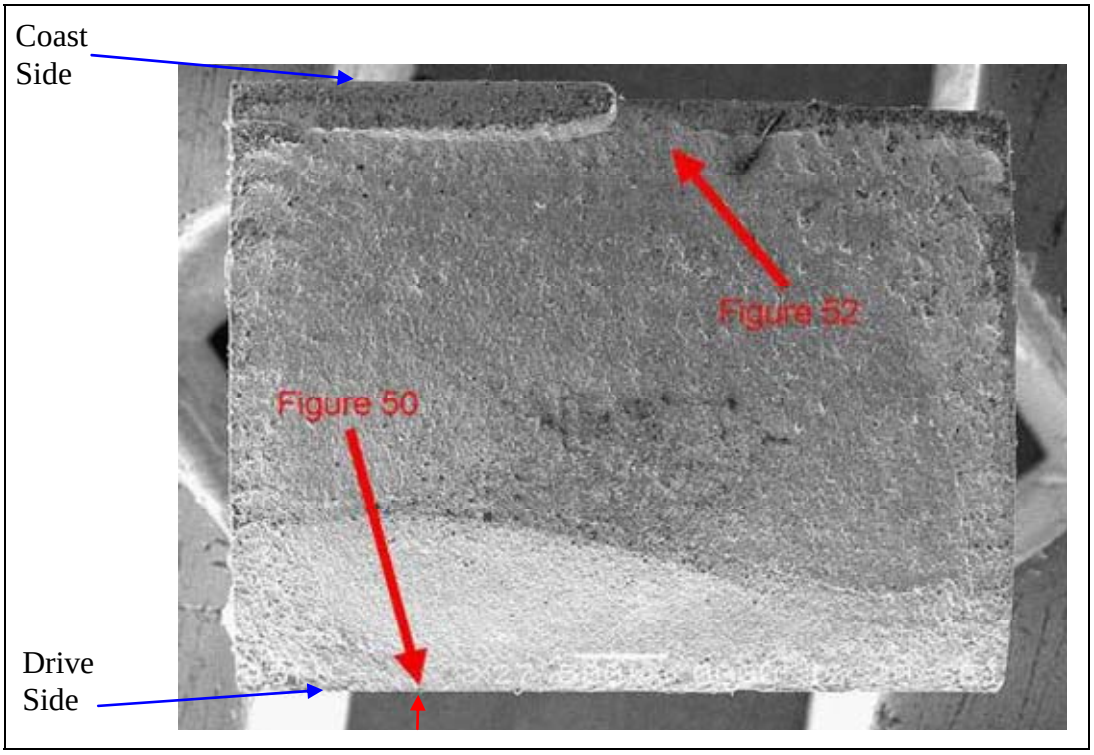

Figure 48. Tooth 28 fracture surface.

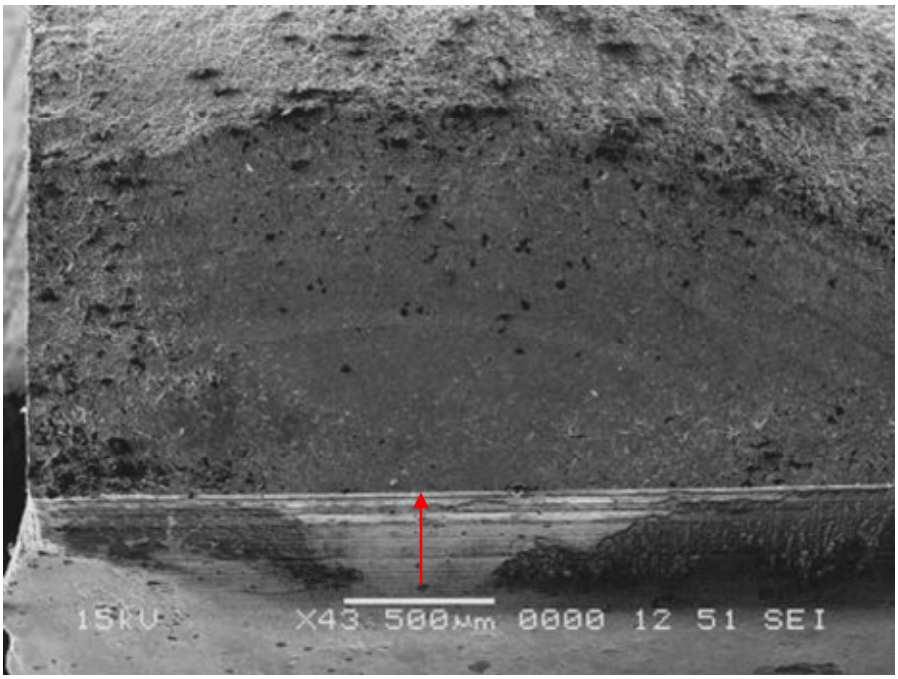

Figure 49. Tooth 28 drive side, primary origin.

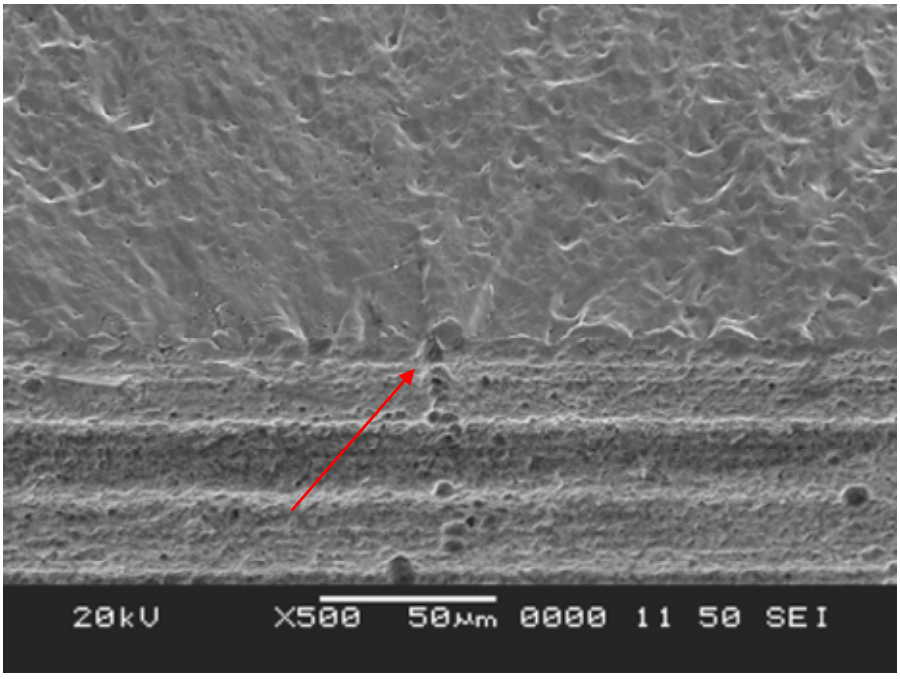

Figure 50. Tooth 28 drive side, primary pit origin.

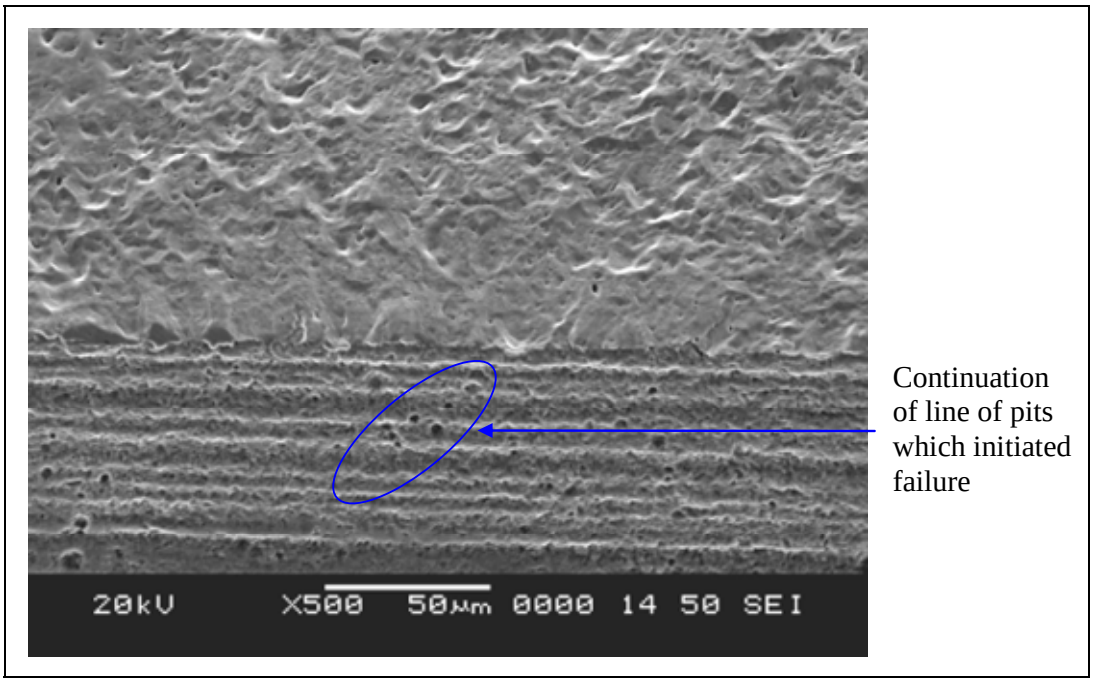

Figure 51. Tooth 28 drive side origin site, gear fracture half.

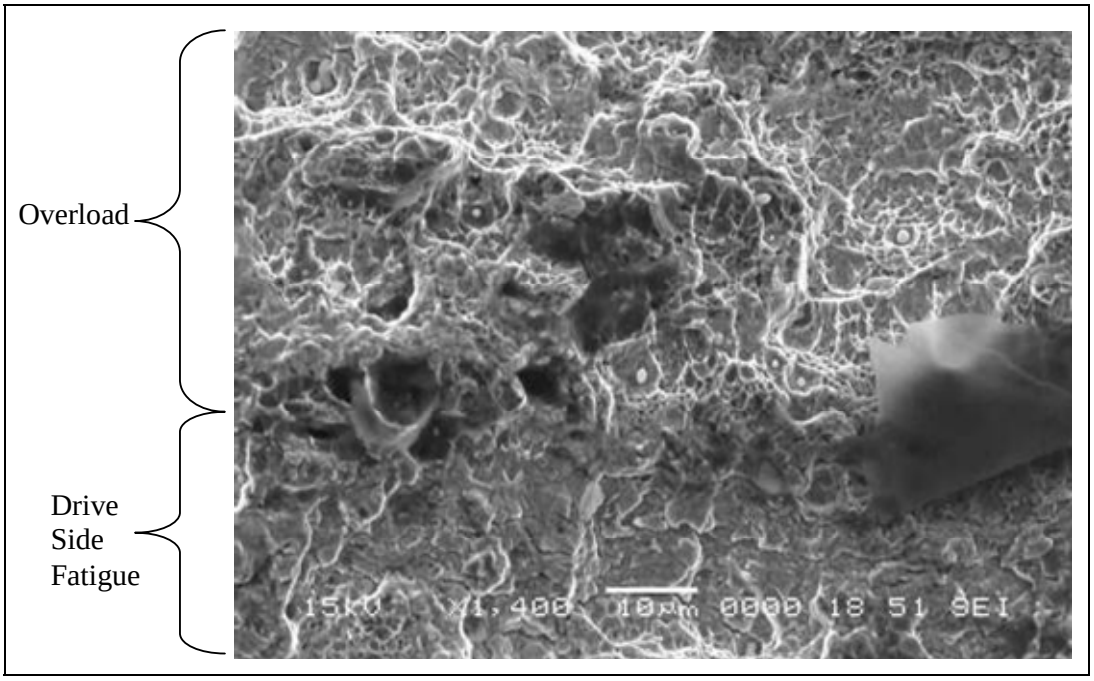

Figure 52. Tooth 28 fracture surface, transition to overload at top.

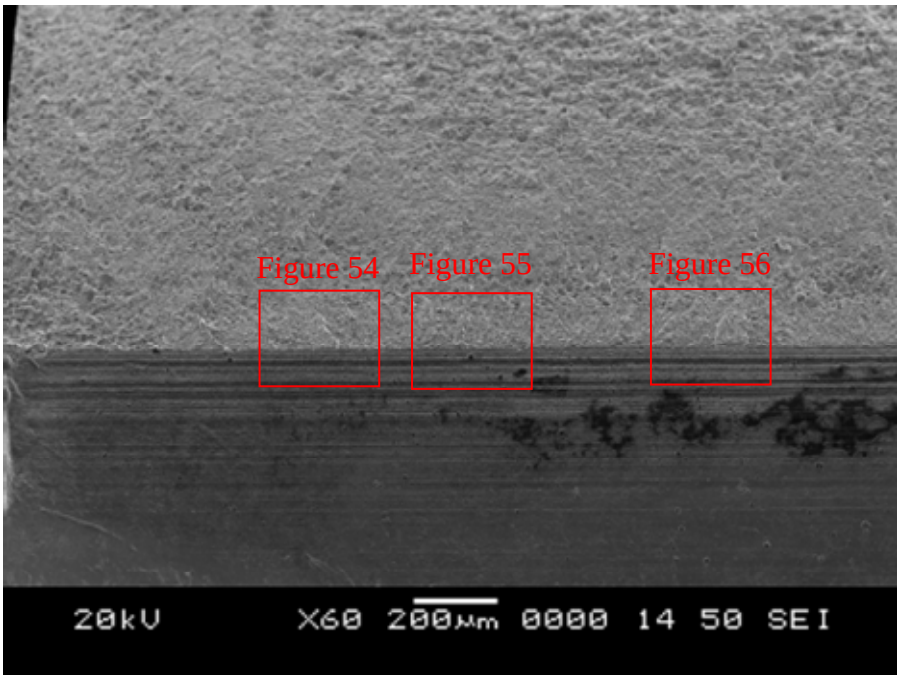

Figure 53. Tooth 29 drive side origin area.

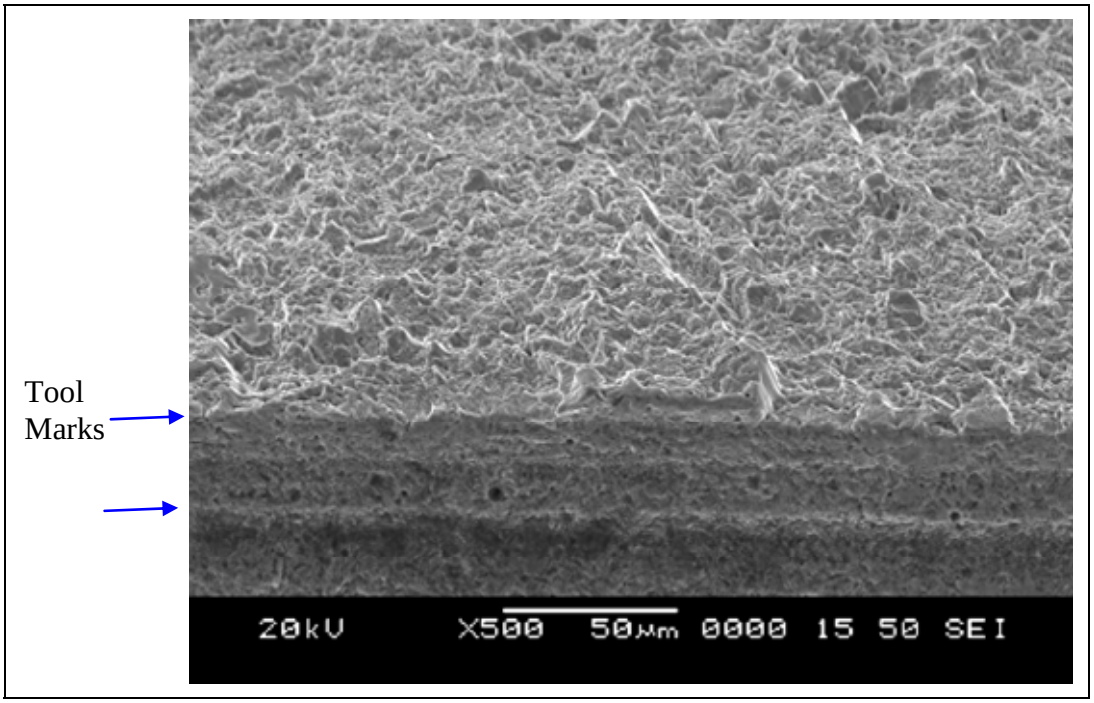

Figure 54. Tooth 29 drive side origin, site no. 1.

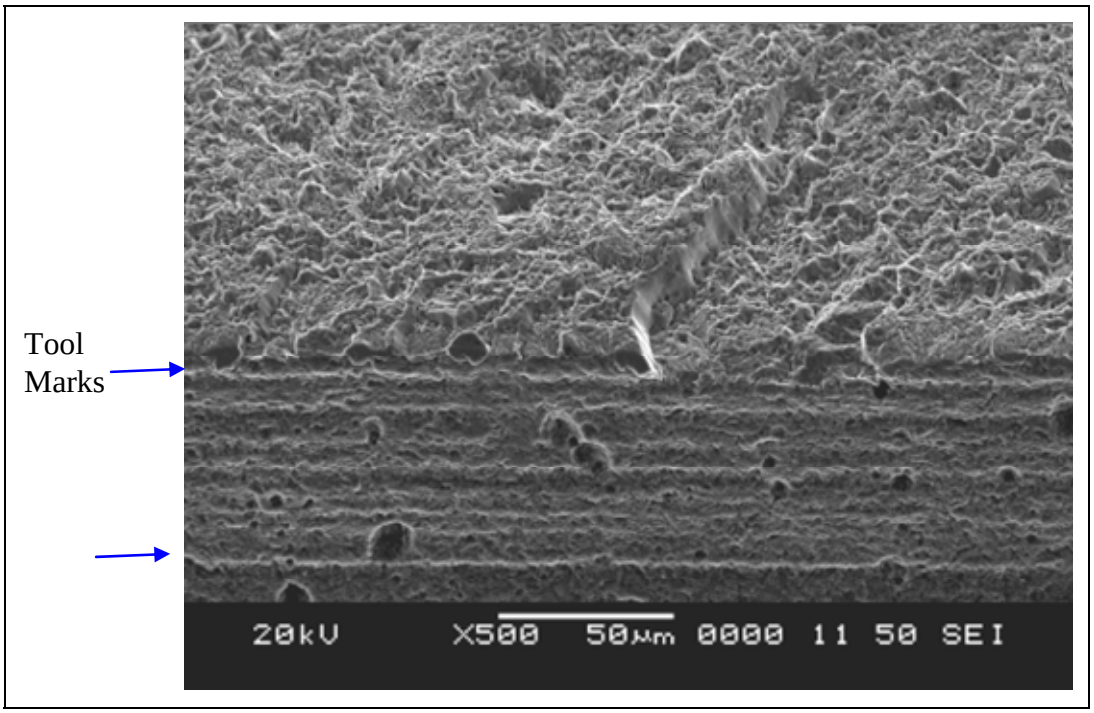

Figure 55. Tooth 29 drive side origin, site no. 2.

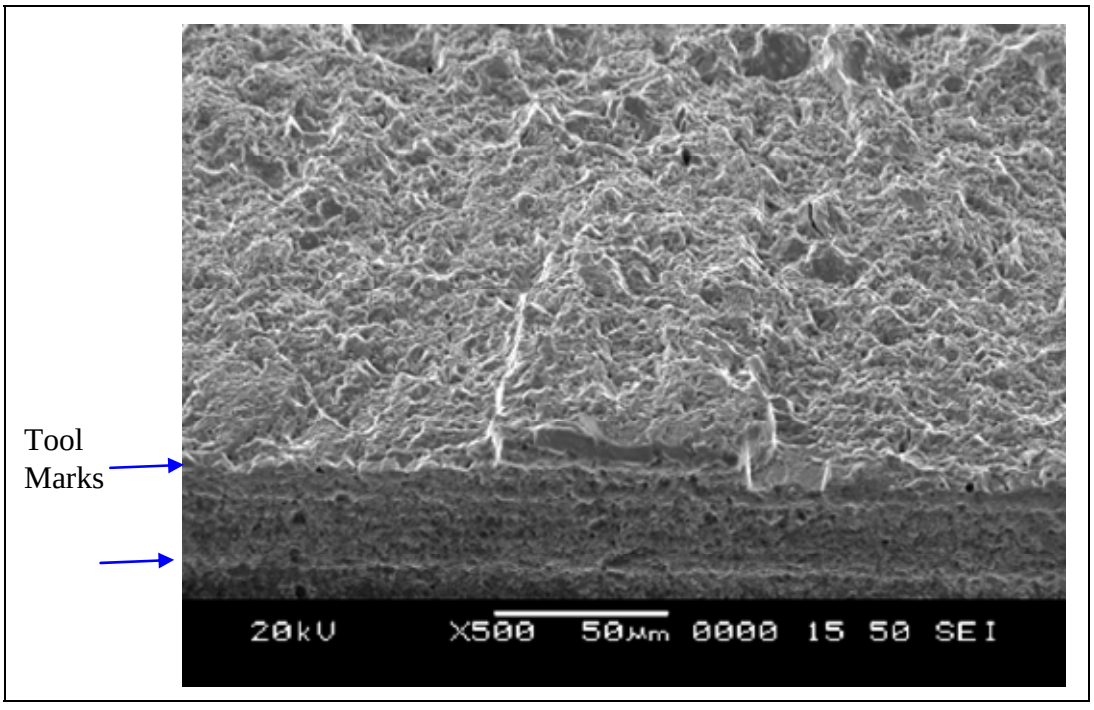

Figure 56. Tooth 29 drive side origin, site no. 3.

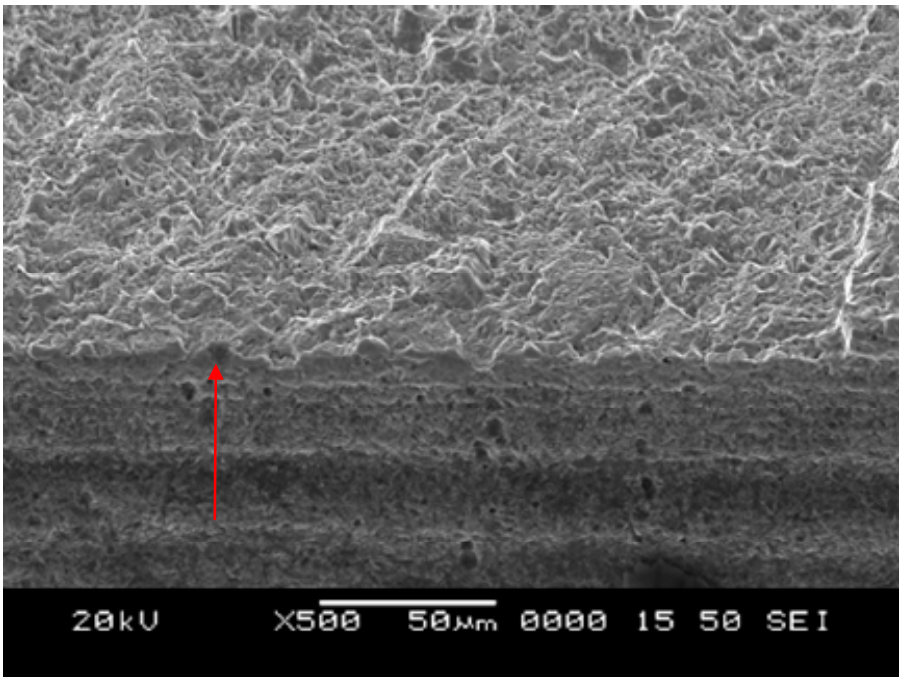

Figure 57. Tooth 29 drive side, primary pit origin.

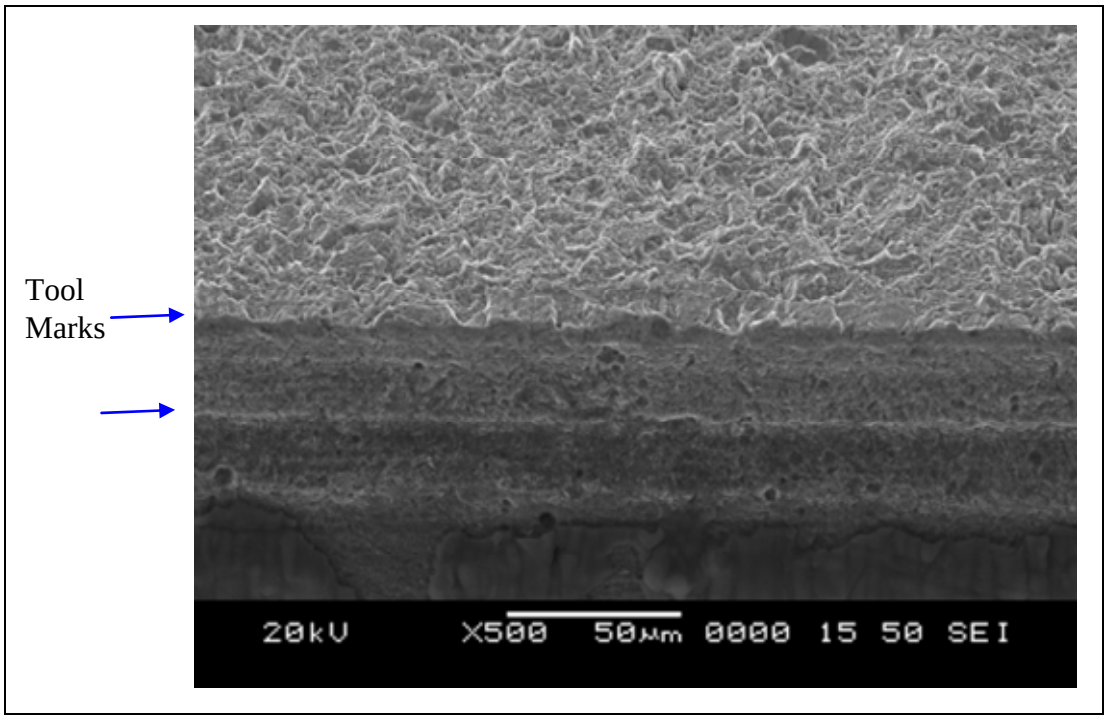

Figure 58. Tooth 29 drive side origin, site no. 4.

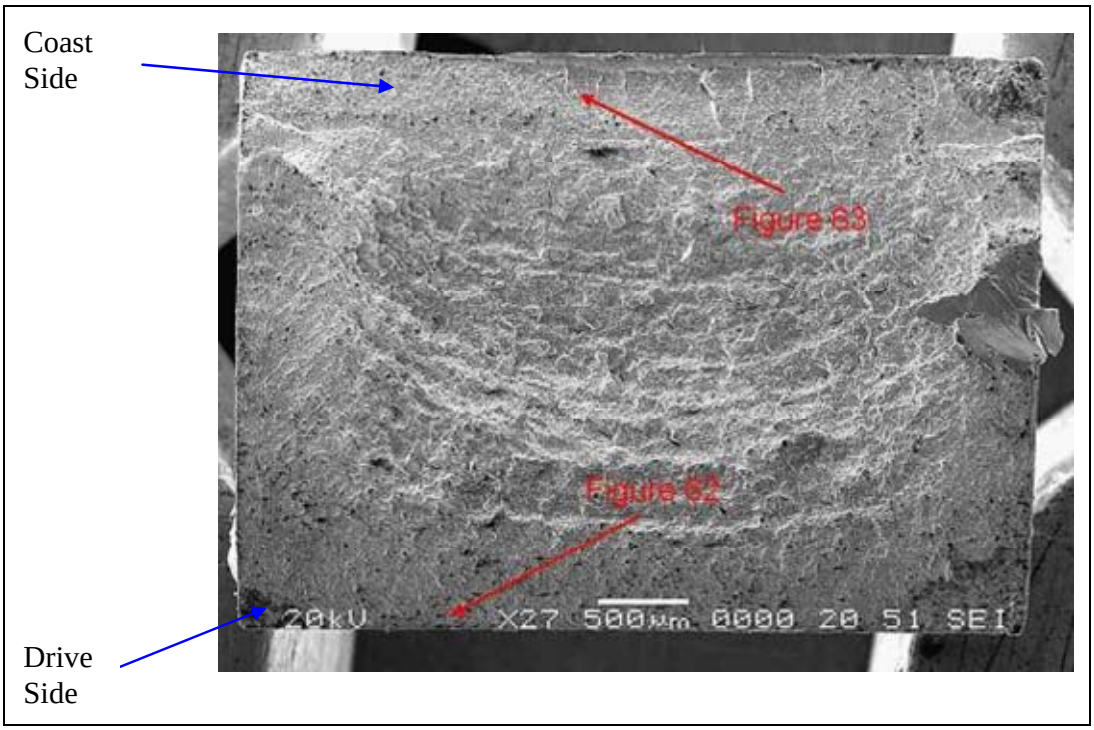

Figure 59. SEM tooth 30 fracture surface.

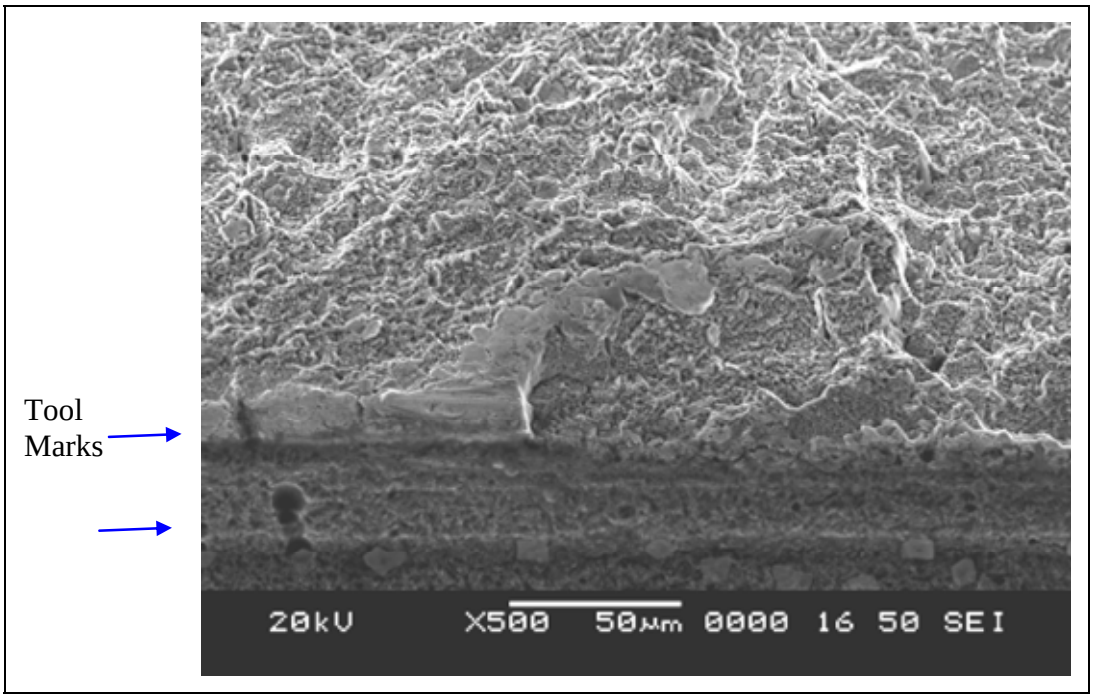

Figure 60. Tooth 30 origin, gear fracture half.

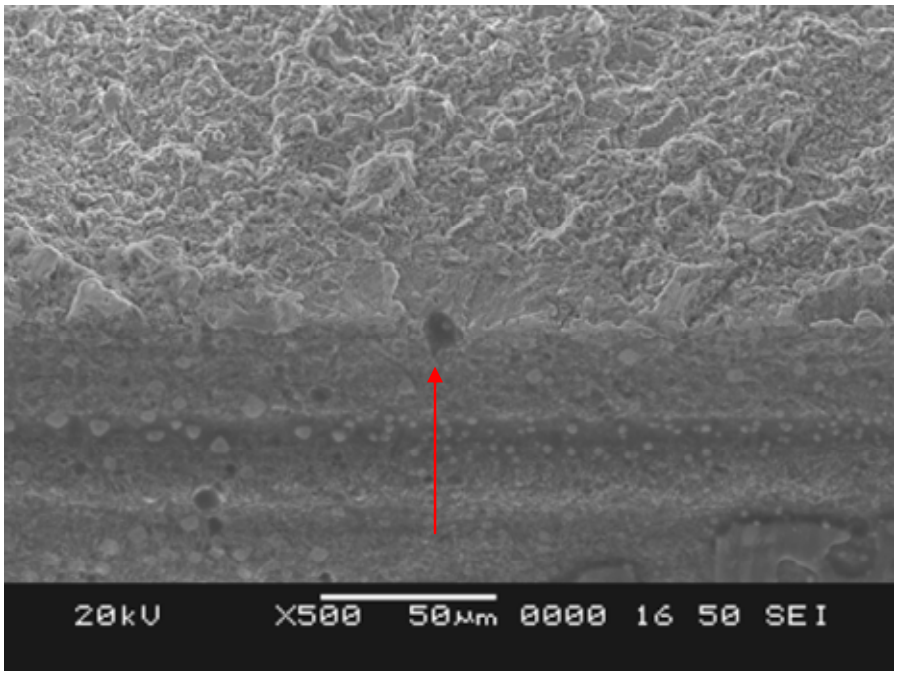

Figure 61. Tooth 30 pit origin, gear fracture half.

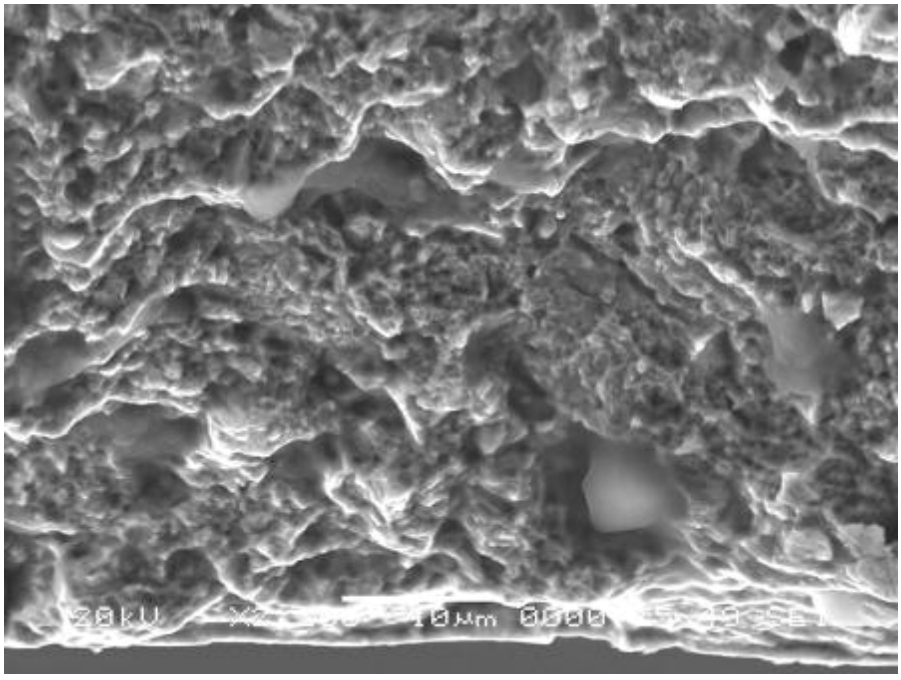

Figure 62. Tooth 30 fracture surface, drive side.

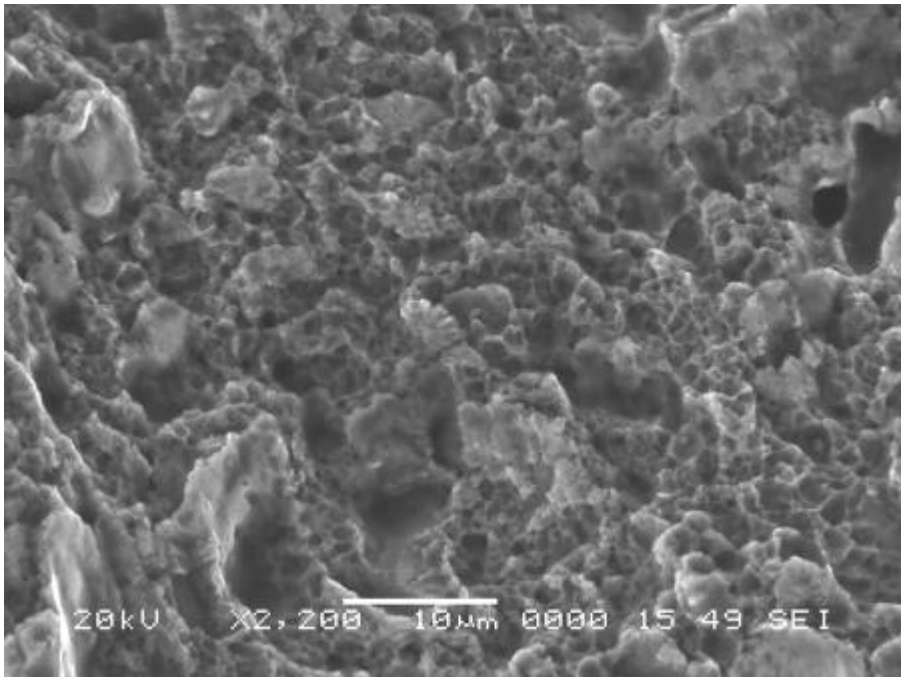

Figure 63. Tooth 30 fracture surface, coast side.

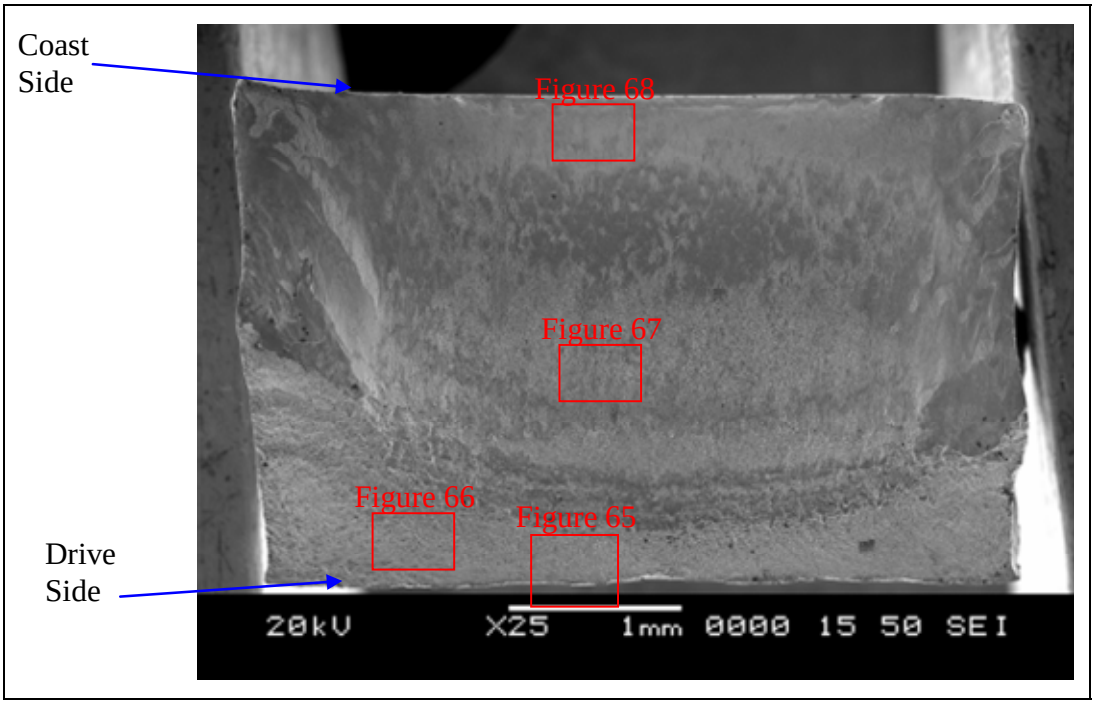

Figure 64. SEM tooth 31 fracture surface.

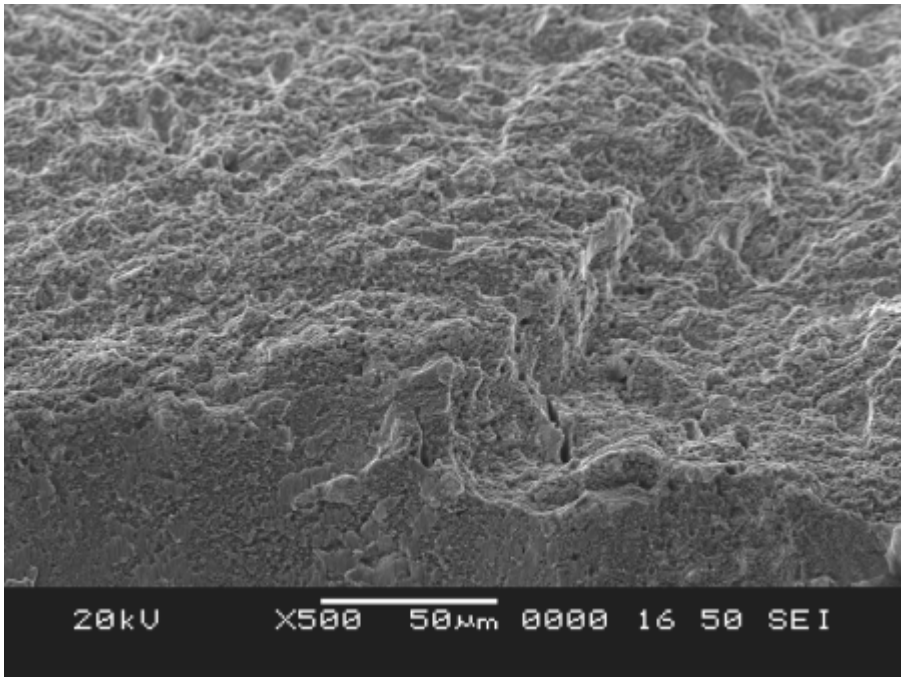

Figure 65. Tooth 31 origin.

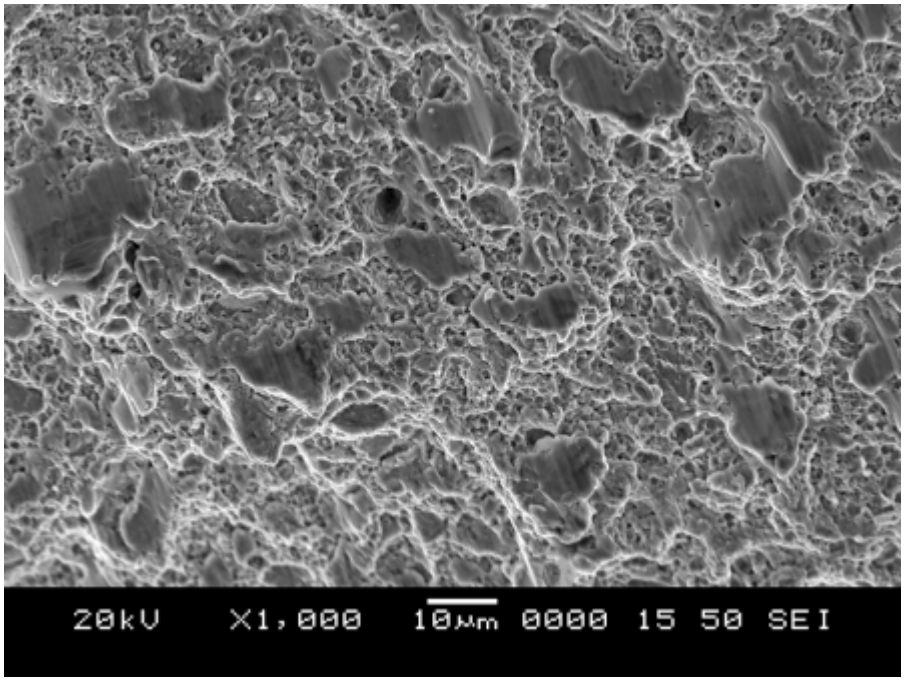

Figure 66. Tooth 31 fracture surface.

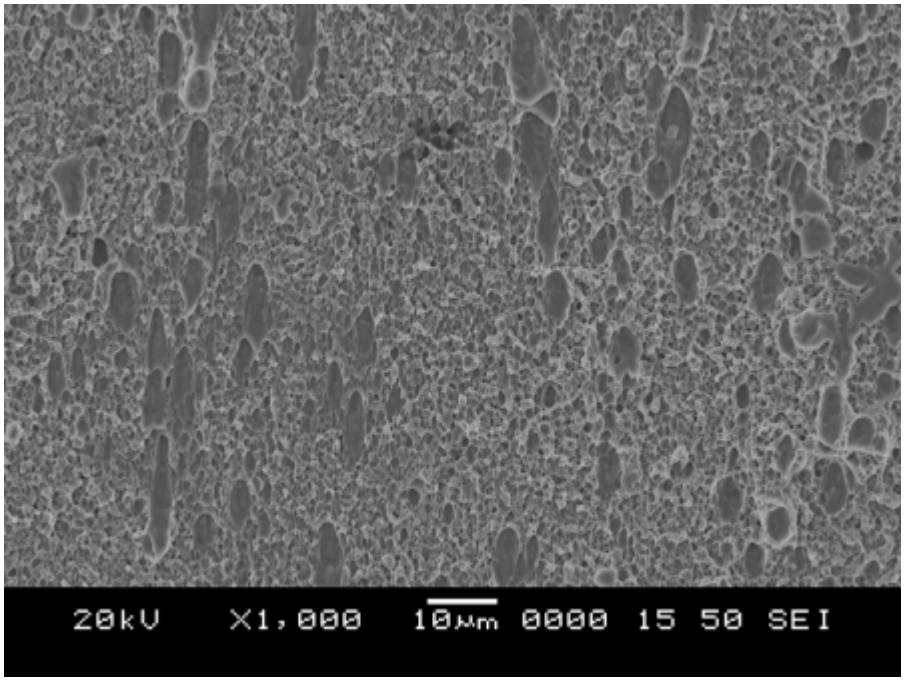

Figure 67. Tooth 31 fracture surface, showing cyclic overload fracture.

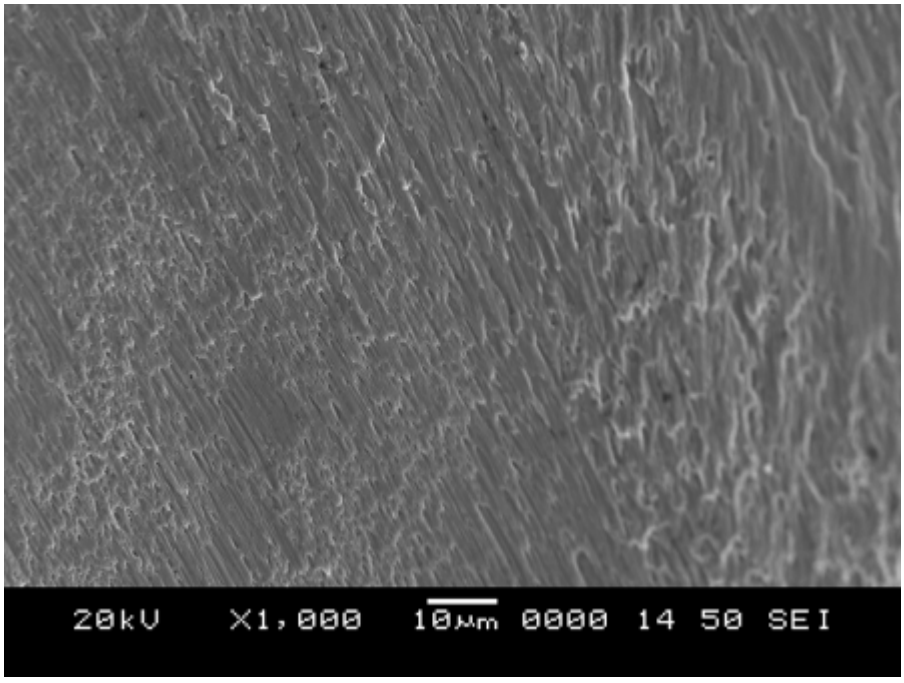

Figure 68. Tooth 31 fracture surface, ductile overload.

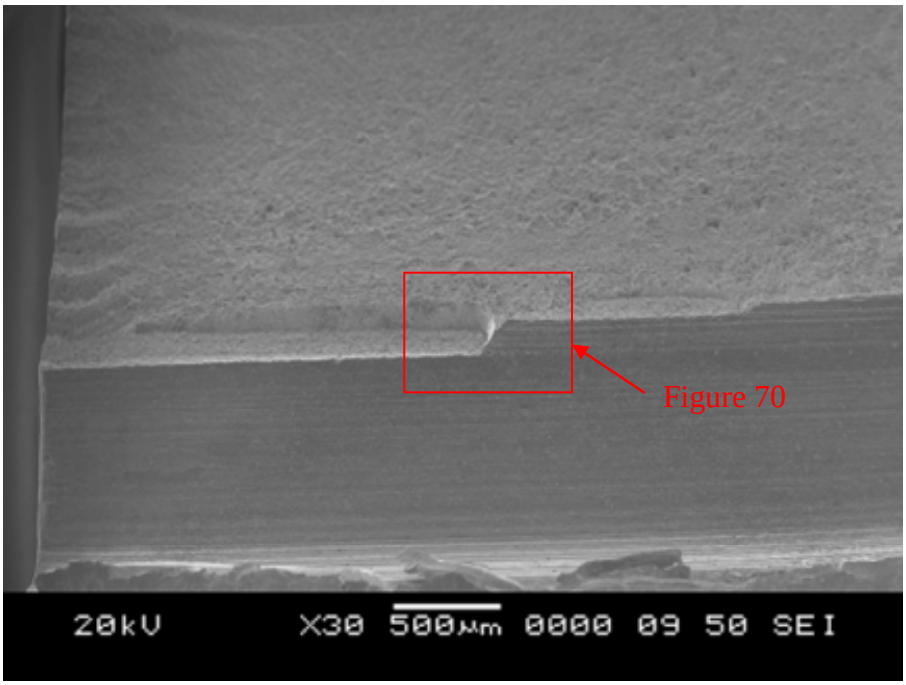

Figure 69. Tool marks, tooth 28 root, gear half.

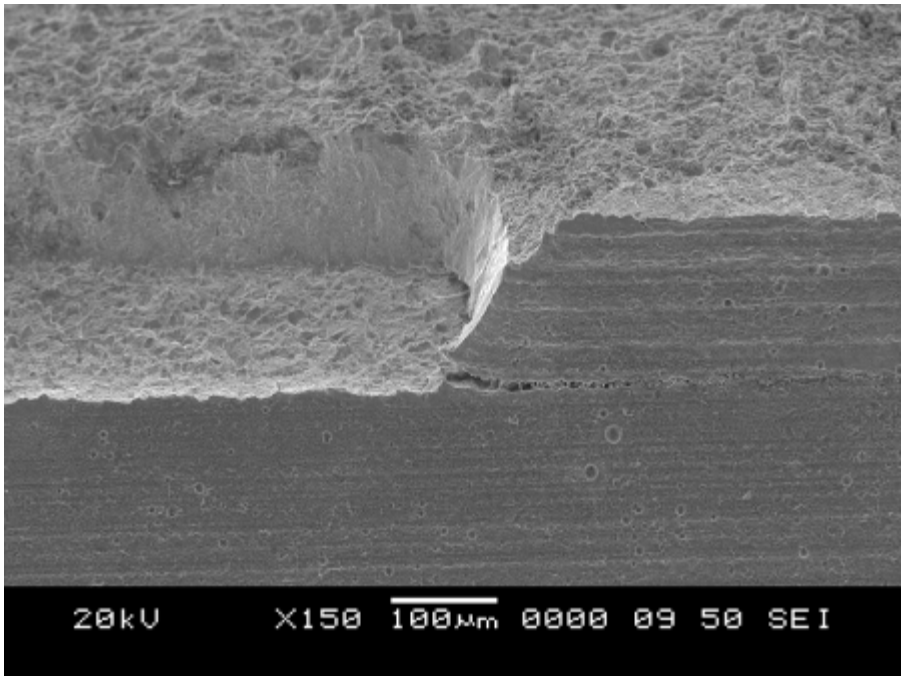

Figure 70. Coast side tool marks, tooth 28 root, gear half. (Note the undercut parallel to tool marks.)

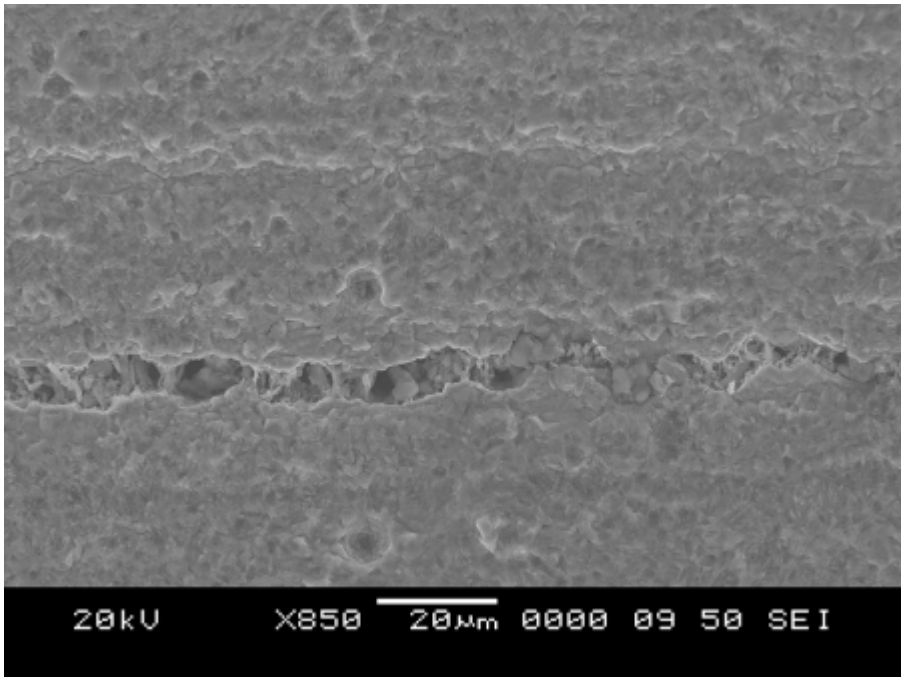

Figure 71. Tooth 28 root, gear half, coast side cracking along tool marks.

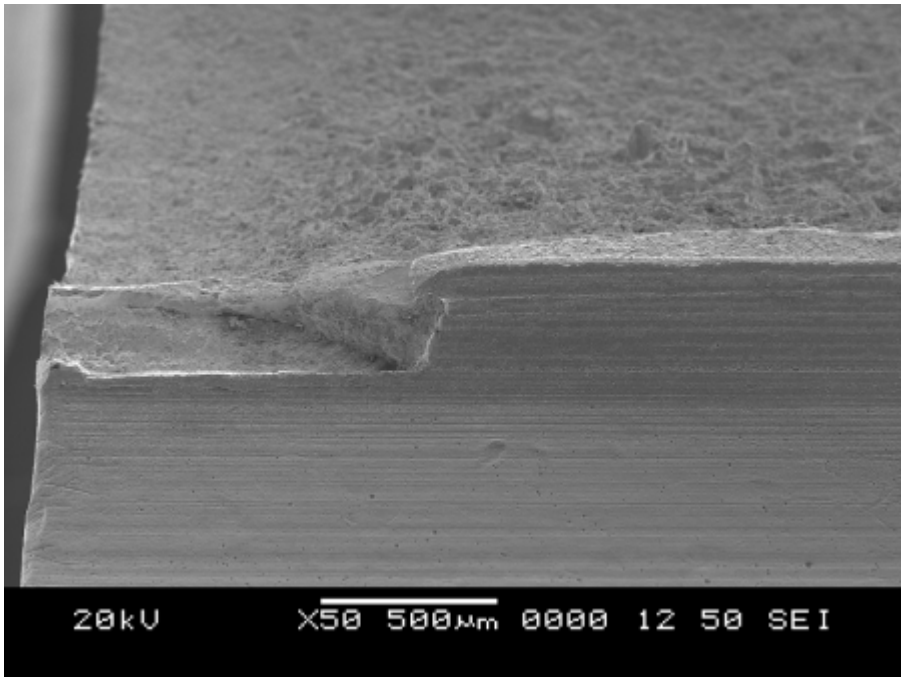

Figure 72. Tooth 29 root, gear half, coast side tool marks.

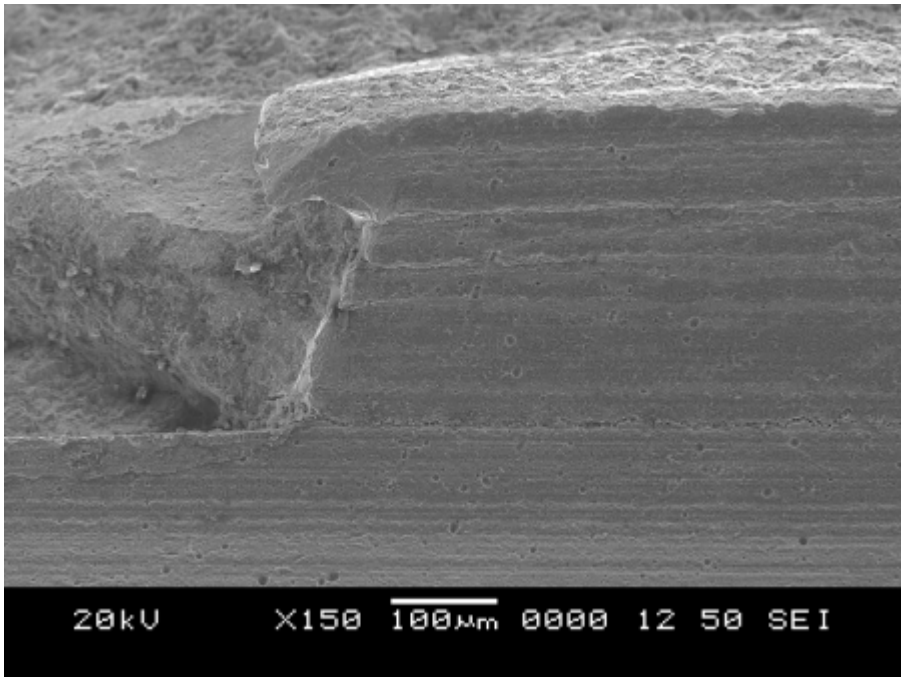

Figure 73. Tooth 29 root, gear half, coast side tool marks.

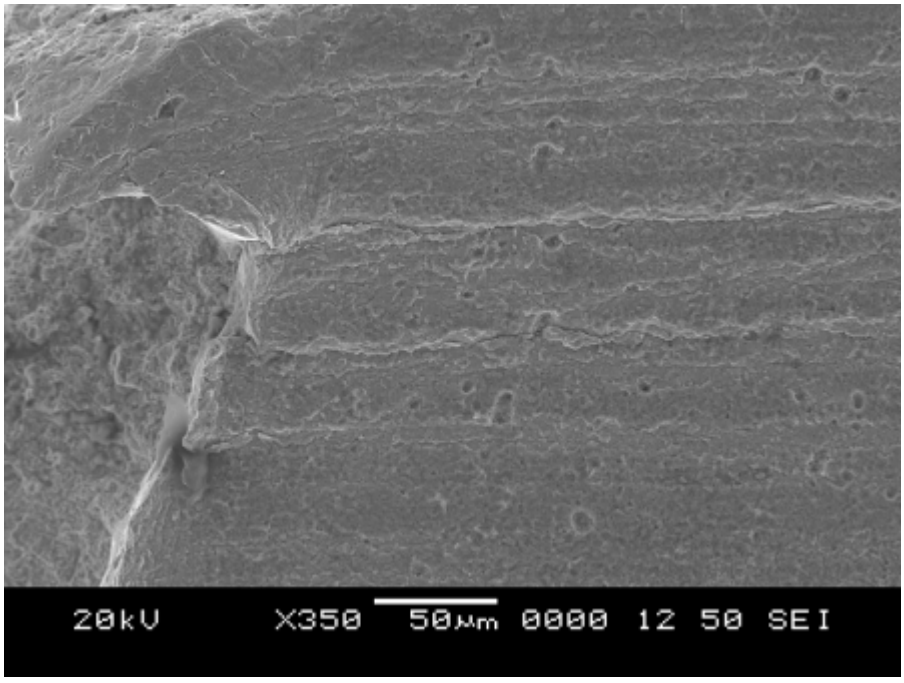

Figure 74. Tooth 29 root, gear half, coast side tool marks, cracking along tool marks.

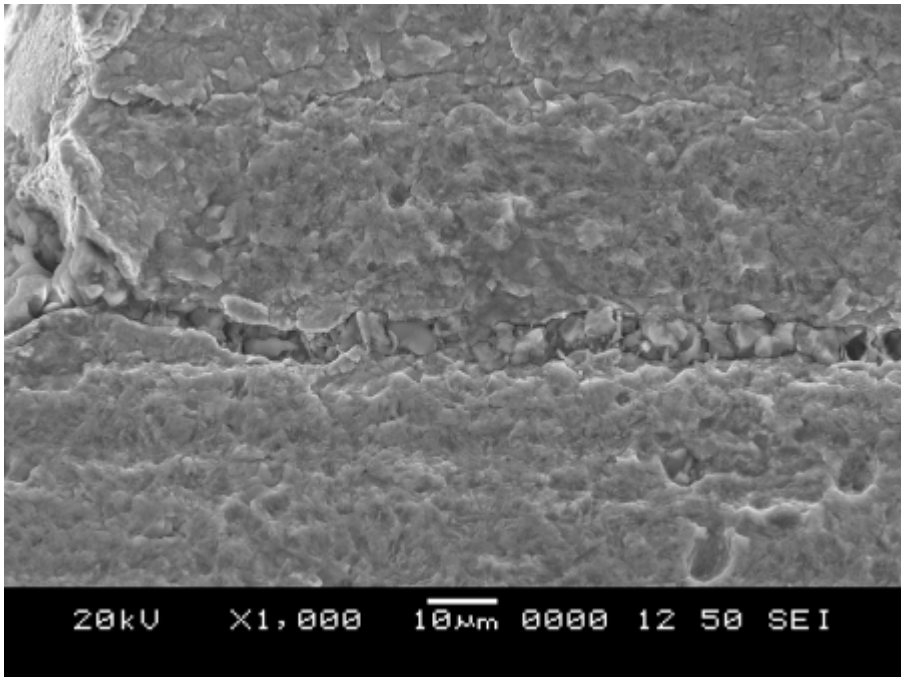

Figure 75. Tooth 29 root, gear half, coast side, cracking along tool marks.

5. Hardness

Hardness measurements were provided by Redstone Technical Test Center. They were made at the tooth root and at the face (near the pitch line) using an Instron Model Tukon 2100 microhardness tester. Effective case depth (EFD) (defined as the depth at which hardness drops to 50 Hardness Rockwell C-scale [HRC]) was found to be approximately 0.026 in at the pitch line and 0.018 in at the root. Hardness data for the profile and root are given in tables 1–3 and shown in figure 76.

Core hardness was measured to be HRC 39.5 using a Wilson Rockwell indenter (Model C524-T). Required minimum core hardness was HRC 30.

Table 1. Hardness measurements, tooth 3, pitch line.

Depth	Knoop Hardness	Rockwell HRC Hardness, Converted	Depth	Knoop Hardness	Rockwell HRC Hardness, Converted
0.002	687	57.8	0.028	500	47.3
0.004	663	56.6	0.030	490	46.7
0.006	651	56.1	0.032	478	45.9
0.008	639	55.4	0.034	468	45.2
0.010	635	55.2	0.036	464	44.9
0.012	628	54.9	0.038	455	44.2
0.014	617	54.3	0.040	455	44.2
0.016	610	53.9	0.042	455	44.2
0.018	590	52.7	0.044	452	44.0
0.020	576	52.0	0.046	446	43.6
0.022	550	50.5	0.048	449	43.8
0.024	542	50.0	0.050	451	43.9
0.026	522	48.8	—	—	—

Table 2. Hardness measurements, tooth 17, pitch line.

Depth	Knoop Hardness	Rockwell HRC Hardness, Converted	Depth	Knoop Hardness	Rockwell HRC Hardness, Converted
0.002	675	57.2	0.028	529	49.2
0.004	662	56.6	0.030	508	47.8
0.006	667	56.8	0.032	483	46.2
0.008	652	56.1	0.034	482	46.1
0.010	633	55.2	0.036	476	45.7
0.012	631	55.0	0.038	464	44.9
0.014	630	55.0	0.040	541	43.9
0.016	614	54.1	0.042	443	43.4
0.018	598	53.2	0.044	457	44.3
0.020	599	53.3	0.046	441	43.2
0.022	587	52.6	0.048	446	43.6
0.024	578	52.1	0.050	446	43.6
0.026	559	51.1	—	—	—

Table 3. Hardness measurements tooth root.

Depth	Knoop Hardness	Rockwell HRC Hardness, Converted	Depth	Knoop Hardness	Rockwell HRC Hardness, Converted
0.002	668	56.9	0.028	466	45.0
0.004	628	54.9	0.030	455	44.2
0.006	627	54.8	0.032	451	43.9
0.008	618	54.3	0.034	446	43.6
0.010	613	54.0	0.036	437	42.9
0.012	598	53.2	0.038	441	43.2
0.014	577	52.1	0.040	442	43.3
0.016	566	51.4	0.042	432	42.5
0.018	549	50.4	0.044	435	42.7
0.020	526	49.0	0.046	421	41.5
0.022	503	47.5	0.048	423	41.7
0.024	501	47.4	0.050	416	41.1
0.026	473	45.5	—	—	—

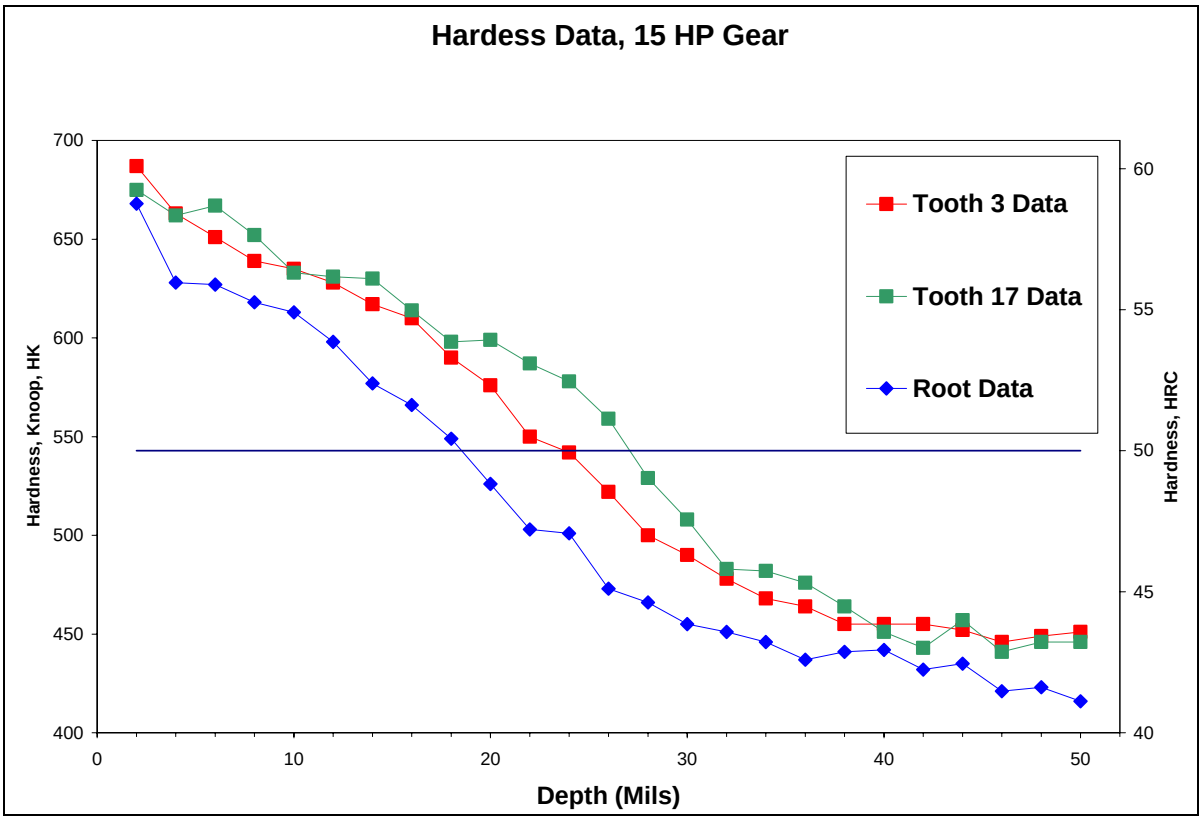

Figure 76. Hardness data tooth and root profiles.

6. Metallography

Cross sections of the gear and two fractured teeth (teeth 28 and 29) were prepared. These were ground and polished through 0.02-μm colloidal silica and subsequently etched with a 2% nital solution. No microstructural abnormalities were observed. Formation of continuous carbide networks was ruled out (figure 77).

7. Edge Break

The edge break for tooth 28 was measured to be 0.0089 in (figure 78). For tooth 29, a value of 0.0088 in (figure 79) was obtained. These values are less than the specified maximum (0.010 in).

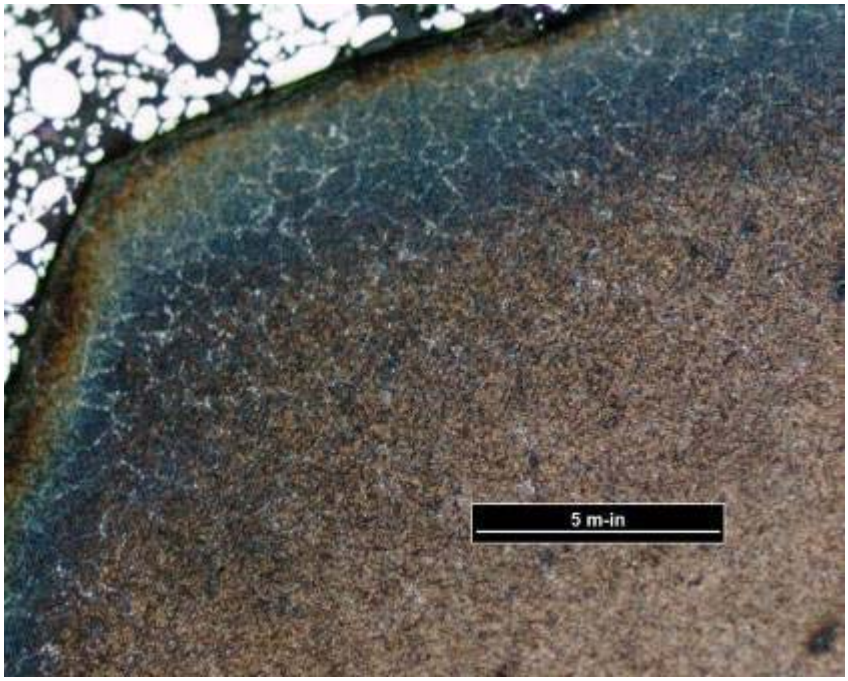

Figure 77. Metallographic cross section demonstrating absence of continuous carbide networks.

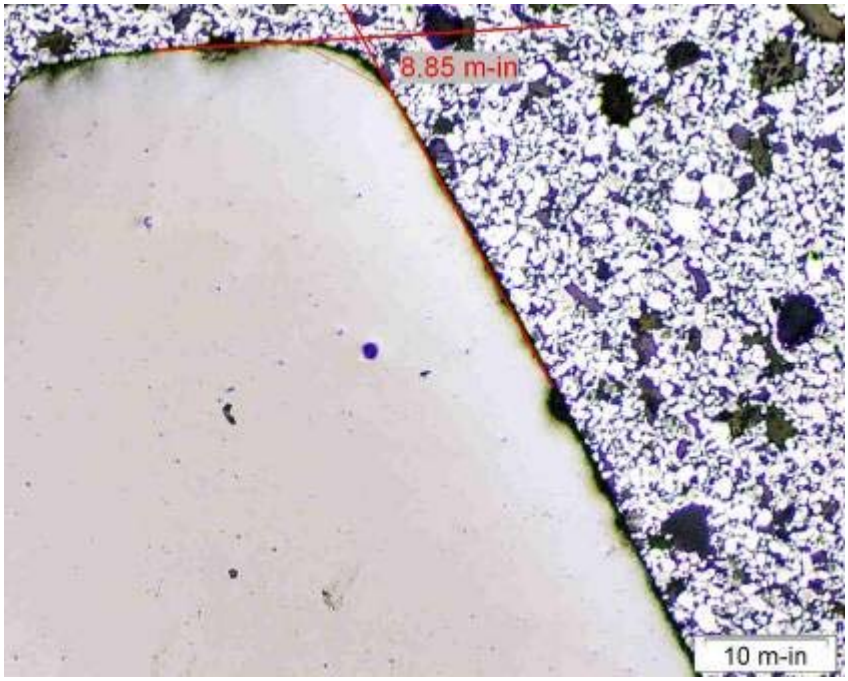

Figure 78. Edge break measurement, tooth 28.

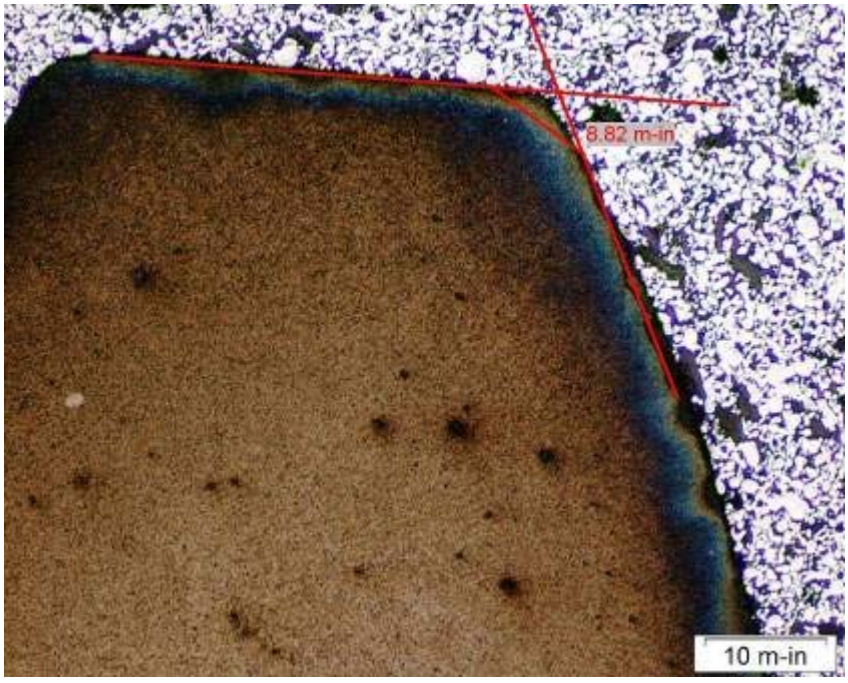

Figure 79. Edge break measurement, tooth 29.

8. Chemical Analysis

Gear chemical composition was analyzed with direct current plasma emission spectroscopy (DC plasma) and combustion infrared detection (carbon and sulfur). The sample was machined prior to testing to remove the carburized case. The results are listed in table 4 along with the chemical composition requirements for the material specified, AMS 6260. The chemical constituency compared favorably with the specification.

Table 4. Chemical composition of 15-hp spare drive gear.

Element	Gear Composition % (by Weight)	AMS 6260 Specification % (by Weight)
Carbon	0.110	0.07–0.13
Manganese	0.61	0.40–0.70
Silicon	0.27	0.15–0.35
Phosphorous	0.023	0.025 maximum
Sulfur	0.021	0.025 maximum
Chromium	1.25	1.00–1.40
Nickel	3.06	3.00–3.50
Molybdenum	0.13	0.08–0.15
Boron	<0.0005	0.001 maximum
Copper	0.32	0.35 maximum

9. Surface Finish

A Taylor-Hobson Form TalySurf Series 2 was utilized to perform laser surface profilometry in a non-worn area of a typical gear tooth. The root mean square (RMS) surface roughness was measured to be 2.85 μm-in (see figure 80). This is well below the specified value (32 μm-in). It must be noted that this measurement was on the surface of a tooth that may have been polished by the mechanical action of the meshing gear teeth during service, although no appreciable wear was observed in the area where the measurement was taken. Additionally, evidence of shot peening was observed (see figure 81). Measurements in the root of the teeth were unobtainable.

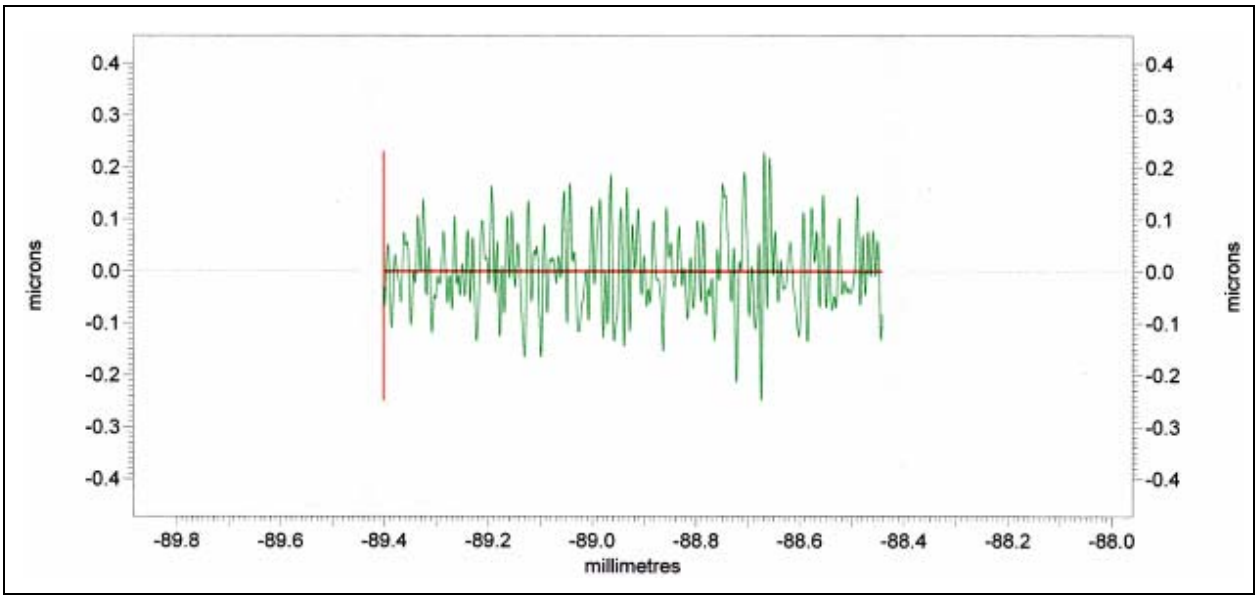

Figure 80. Surface roughness measurement.

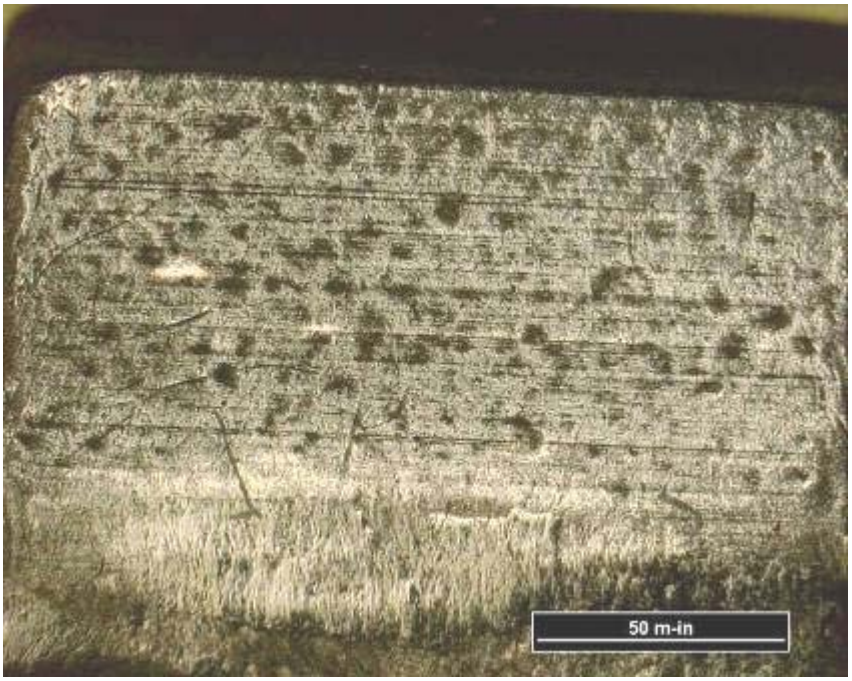

Figure 81. Optical photograph of shot peened surface finish.

10. Residual Stress

The residual stress was measured in the hoop (or rotational) direction on the non-worn areas on the coast side of teeth 28 and 29 which were separated from the gear during fracture. Compressive stresses of 114.4 and 125.5 ($\pm$ 2.6 ksi) were obtained. The difference between the measurements is likely due to experimental errors caused by small sample size and the slight curvature of the measured surface. However, the reported stresses compare favorably with other shot peened helicopter gears, such as the Blackhawk spiral bevel gear.

11. Recommendations

- Identify and eliminate the source of the pitting.
- Eliminate or reduce the magnitude of the tool marks present in the tooth root fillet.

12. Conclusions

Gear failure resulted from bending fatigue failure of two primary teeth. Failure of these teeth initiated a sequence (in two separate groups) of increasingly faster bending fatigue tooth failures. Failure progressed in the order of meshing for both groups. Ultimately, transmission error became so large that the gears did not mesh properly, causing rapid stripping of the remaining teeth and damage to the pinion teeth as well.

The two groups of bending fatigue failure sequences were identified as teeth 1, 2, 3, and 4 and teeth 28, 29, 30, and 31. Identical four tooth failure sequences have been found on other failed spare drive gears. However, this is only gear where two such sequences have been identified.

Primary origins for all bending fatigue failures were located at the drive side root near the area of highest stress. This high stress point had been previously established by finite-element analysis at U.S. Army Aviation and Missile Command.

Pits were found at the primary origins of the initial teeth (tooth 1 and tooth 28) in each of the bending fatigue failure sequences. A pit of approximately 10 μm was found at the primary origin.

The EFD was determined to be 0.018 in at the root and 0.026 in at the pitch diameter. The EFD was defined as the depth at which a value of 50 HRC is obtained.

No inherent microstructural abnormalities were observed, such as continuous carbide networks, but significant tool marks and pits were found on the exterior surface at or near the fracture origins.

The edge breaks were found to be within specification (0.010 in maximum) for tooth 28 (0.0089 in) and tooth 29 (0.0088 in).

Chemical testing confirmed that the gear was made from AMS 6260 alloy steel in accordance with drawing material requirements.

The surface finish was estimated to be 2.85 μm-in, RMS. This is within the drawing specification (32 μm-in maximum). However, tool marks were observed near the roots of gear teeth.

Residual stresses were measured on the coast side of two teeth that separated from the gear. The resulting residual stresses were comparable to other shot peened 6260 material.

NO. OF
COPIES ORGANIZATION

1 (PDF ONLY) DEFENSE TECHNICAL INFORMATION CTR
DTIC OCA
8725 JOHN J KINGMAN RD
STE 0944
FORT BELVOIR VA 22060-6218

1 US ARMY RSRCH DEV & ENGRG CMD
SYSTEMS OF SYSTEMS INTEGRATION
AMSRD SS T
6000 6TH ST STE 100
FORT BELVOIR VA 22060-5608

1 INST FOR ADVNCD TCHNLGY
THE UNIV OF TEXAS
AT AUSTIN
3925 W BRAKER LN
AUSTIN TX 78759-5316

1 DIRECTOR
US ARMY RESEARCH LAB
IMNE ALC IMS
2800 POWDER MILL RD
ADELPHI MD 20783-1197

3 DIRECTOR
US ARMY RESEARCH LAB
AMSRD ARL CI OK TL
2800 POWDER MILL RD
ADELPHI MD 20783-1197

ABERDEEN PROVING GROUND

1 DIR USARL
AMSRD ARL CI OK TP (BLDG 4600)